Ann. Rev. Nucl. Part. Sci. 1987. 37: 133–76

ELECTRON SCATTERING AND NUCLEAR STRUCTURE

Bernard Frois

Service de Physique Nucleaire–Haute Energie, CEN Saclay, 91191 Gif-sur-Yvette Cedex, France

Costas N. Papanicolas

Department of Physics and Nuclear Physics Laboratory, University of Illinois, Urbana, Illinois 61801, USA

CONTENTS

0163–8998/87/1201–0133$02.00

1. INTRODUCTION

Traditional nuclear models attempt to explain nuclear structure in the framework of nucleonic degrees of freedom only. The interaction between nucleons is described in terms of an effective potential whose microscopic origin would be found in the suppressed degrees of freedom. The properties of the nucleon are assumed to be the same in the nuclear medium as in vacuo. Until quite recently, this simple description was found satisfactory for most nuclear observables.

During the last five years the limits of this framework have been carefully mapped by electron scattering experiments. For heavy nuclei, the mean field theory based on phenomenological effective interactions provides a reliable and consistent description. However, its shortcomings have been clearly seen. In few-body systems, the discrepancies between NN potential theory and experiment are dramatic. The explicit introduction of non-nucleonic degrees of freedom has been demonstrated to be essential.

The scarch for the appropriate degrees of freedom to describe nuclei is the central focus of nuclear physics today. Therefore we explore in this review our current understanding of nuclear structure as defined by electromagnetic data. The precision of the electromagnetic probe allows us to define accurately the limits of present theoretical descriptions. We review here a broad range of subjects that have been addressed by recent experiments, from the study of meson exchange currents and single-particle distributions to collective excitations in heavy nuclei. However, we do not discuss elastic magnetic scattering, inelastic excitation of discrete states, or single-nucleon knockout reactions since these reactions were recently reviewed (1–3). The principal aim of this review is to offer a fresh perspective on nuclear structure, based on the new generation of electron scattering data presented here and in the above-mentioned articles.

2. ELECTRON-NUCLEUS SCATTERING

2.1 *The Role of Electron Scattering*

Electron scattering offers unique and widely appreciated advantages for the study of nuclear structure—the weakness of the interaction and the knowledge of the reaction mechanism being the most significant. Multiple scattering effects are negligible and perturbation of the initial state of the nucleus is minimal. The ability to vary independently the momentum and the energy transferred to the nucleus allows the mapping of spatial distributions of the constituent particles. Because electrons are point particles, they offer superb spatial resolution that can be adjusted to the scale of processes that need to be studied. This scale is related to the momentum transfer $q(\lambda\!\!\!^{-} \approx 1/q)$. Incident electron energies of 500 MeV result in res-

olution of the order 0.5 fm, which is ideally suited for the study of nucleon distributions in nuclei. At much higher energies, $E \geq 10$ GeV, electrons have a spatial resolution sufficient to probe quark distributions.

Considerable experimental difficulties had to be overcome in order to exploit the potential of this probe of nuclear structure. One needs to map out form factors to sufficiently high momentum transfers in order to bring out the details of nuclear charge and magnetization densities. Since form factors of heavy nuclei decrease rapidly as a function of momentum transfer, measurements of very small cross sections are imperative. Huge magnetic spectrometers of large solid angle, wide momentum acceptance, and intense electron beams are needed. The difficulty is increased by the need to isolate specific nuclear excitations. An energy resolution $\Delta E/E = 10^{-4}$ is barely sufficient for nuclear studies. Such experimental constraints led to the development (starting around 1970) of a completely new design for experimental facilities. The detection and data acquisition systems met these requirements in the mid-1970s, permitting for the past ten years the exploitation of the possibilities of electron scattering for nuclear studies.

2.2 *The Nuclear Response*

In electron scattering the incident electron transfers momentum $\mathbf{q}$ and energy ω to the nucleus, and is scattered to an angle θ. In inclusive experiments, the final state of the nucleus is not known. In exclusive experiments, specific channels of the final state are selected and studied. When there are more than two particles in the final state, this necessitates the coincident measurement of some of the products of nuclear deexcitation.

Schematic views of the cross sections of electron-nucleus and electron-nucleon scattering as functions of the energy transfer ω for a fixed momentum transfer $\mathbf{q}$ are shown in Figure 1. The low energy, low momentum transfer region corresponds to conventional nuclear spectroscopy. The first peak is due to elastic scattering from the ground state, it is followed by the low-lying excited states and the giant multipole resonances. At larger energy transfers, the cross section increases and has a smooth ω dependence. This is the region of "continuum" excitation. The cross section reaches a maximum in the region $\omega \approx q^2/2M_{\text{nucleon}}$ corresponding to "quasielastic scattering" from individual nucleons. The nuclear quasielastic peak is followed at higher energy transfers by successive broad peaks due to the nucleon resonances. At the limit where both q and ω become very large, one reaches the region of scattering by nucleon constituents. This is the region where evidence for pointlike particles, partons, has been found by scale invariance. In this region, a difference in the scaling behavior between iron and deuterium (4) was recently observed, the so-called EMC effect, named after the European Muon Collaboration (EMC) that first identified it.

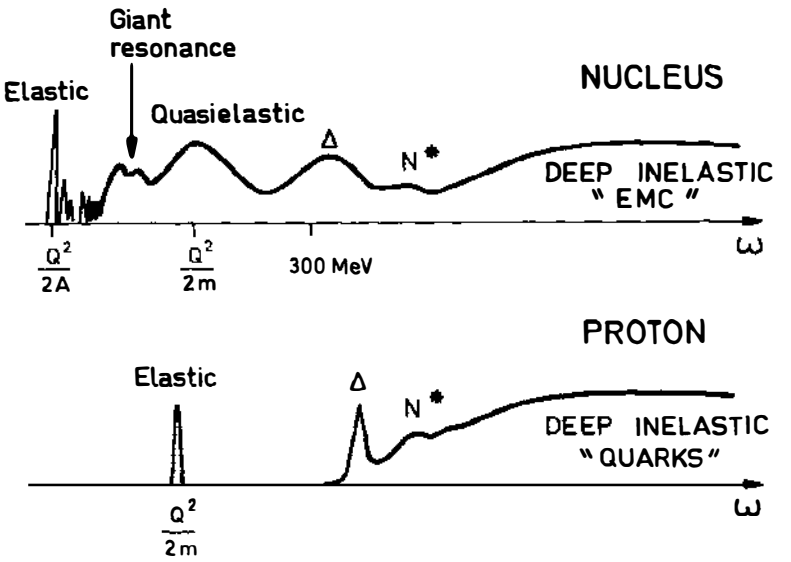

Figure 1 Schematic shape of electron-nucleus and electron-nucleon cross sections as a function of the energy transfer ω.

The comparison in Figure 1 between electron scattering from a nucleus and from the proton shows the striking difference arising from the influence of the nuclear medium.

2.3 *Formalism*

We present here only the basic definitions necessary for discussing electron scattering from nuclei in the one-photon-exchange approximation. More extensive treatments of the formalism can be found elsewhere (5–8).

For an unpolarized incident elcctron beam, the inclusive electron-nucleus cross section is the sum of two terms,

$$\frac{\mathrm{d}^2\sigma}{\mathrm{d}E'\,\mathrm{d}\Omega} = \sigma_{\mathrm{Mott}}\left[\left(\frac{q_\mu^4}{\mathbf{q}^4}\right)R_{\mathrm{L}}(q,\omega) + \left(-\frac{1}{2}\frac{q_\mu^2}{\mathbf{q}^2} + \tan^2\frac{\theta}{2}\right)R_{\mathrm{T}}(q,\omega)\right], \qquad 1.$$

where σ_{Mott} is the point charge electron scattering cross section, given by

$$\sigma_{\mathrm{Mott}} = \left[\frac{\alpha\cos\theta/2}{2E\sin^2\theta/2}\right]^2; \qquad 2.$$

$R_{\mathrm{L}}(q,\omega)$ and $R_{\mathrm{T}}(q,\omega)$ are the longitudinal and transverse response functions; and q^μ is the four-momentum of the exchanged virtual photon:

$$q^\mu = (\omega, \mathbf{q}) \qquad q = |\mathbf{q}|. \qquad 3.$$

Neglecting the electron mass, q^μ and ω are given by

$$Q^2 = -q_\mu^2 = -4EE' \sin^2 \frac{\theta}{2} \qquad \omega = E - E' \qquad 4.$$

$$q_\mu^2 = \omega^2 - q^2 \leq 0. \qquad 5.$$

E and E' are the energies of the incident and scattered electron; θ is the electron scattering angle (Figure 2), all quantities being measured in the laboratory frame.

As indicated in Equation 1, by selecting the kinematic conditions one can vary the polarization of the virtual photons and can separate the longitudinal and transverse response functions. One performs a combination of forward and backward measurements, keeping the value of the momentum transfer fixed by varying the incident electron energy. The response functions $R_L(q,\omega)$ and $R_T(q,\omega)$ contain the information on the structure of charge and current distributions in the nucleus.

3. FEW-NUCLEON SYSTEMS

A basic goal of nuclear physics, the exact description of finite nuclei in terms of a realistic nucleon-nucleon interaction, is at present beyond the reach of theory. Drastic approximations have to be made to solve the nuclear many-body problem. It is only for few-nucleon systems, $A = 2$ and $A = 3$, that one has found exact solutions in a nonrelativistic framework. Thus, the experimental study of these systems is essential in order to explore the limits of the mesonic description of the nucleon-nucleon interaction. The electromagnetic properties of the two- and three-nucleon systems are of particular interest. Experimental progress has been considerable in the last five years. The form factors of the deuteron, of tritium, and of ^{3}He have been accurately determined up to 1 $(\text{GeV}/c)^2$. These new

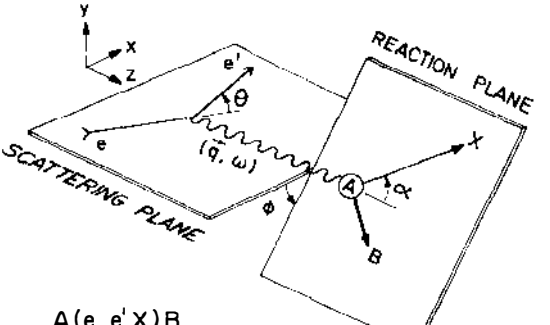

Figure 2 Kinematical definitions for coincident electron scattering in the one-photon-exchange approximation.

data offer a rich testing ground for theory and have thoroughly explored the character of meson exchange currents in few-nucleon systems.

3.1 *Meson Exchange Currents*

The importance of meson exchange currents in electromagnetic data was realized (9) shortly after the pion was discovered. Such currents are required by electromagnetic gauge invariance as well as other considerations based on current algebra and chiral symmetry. However, no conclusive evidence for their presence was available at that time. The large coupling constants associated with meson-nucleon vertices do not allow the derivation of a convergent diagrammatic expansion. The inclusion or omission of specific diagrams changes the interpretation of experimental data. Chemtob & Rho (10), by highlighting the role of chiral symmetry, have identified a clear hierarchy of dominant processes where the pion plays a central role. The description of the π exchange current is constrained by model-independent theorems, valid for "soft pions" that have small momenta at the scale of the nucleon mass. The first investigations of the effects of mesons in nuclei have relied on these model-independent predictions. The classical example is the slight increase observed in the thermal neutron capture by the deuteron. Riska & Brown (11) showed that the 10% disagreement between experiment and theory was the signature of the π exchange current. Various experimental results have now clearly demonstrated that low energy theorems are operative in nuclei (12).

It is crucial to investigate the validity of mesonic theory as a function of momentum transfer in order to find the momentum at which it begins to break down. This is precisely what has been accomplished by electron scattering experiments in the last decade.

3.2 *Electrodisintegration of the Deuteron at Threshold*

This M1 isovector transition is an admixture of two amplitudes, the $^3S_1$ and the $^3D_1$ components of the ground-state wave function of the deuteron coupled to the $^1S_0$ state of the n-p system. It is the inverse reaction of the neutron capture $n+p \rightarrow D+\gamma$. In thermal neutron capture, the pion has negligible momentum and the contribution of the π exchange current is given in a model-independent way by low energy theorems. In the electrodisintegration of the deuteron at threshold, the spatial distribution of meson exchange currents can be explored with virtual photons of adjustable wavelength. The nucleonic and mesonic currents contributing to the cross section have strong destructive interferences that occur successively at different momentum transfers (13). Thus, measurements at specific momentum transfers isolate the contributions from different meson exchange processes (14, 15).

Cross sections for this reaction have been measured up to 28 fm^{-2}. Experimental data (13), averaged over the energy of the n-p system near threshold ($E_{np} \leq 3$ MeV), are shown in Figure 3, together with theoretical predictions using the Paris potential (15). The predictions take into account the effect of both nucleons and mesons. The purely nucleonic contribution has a deep minimum around $Q^2 = 12$ fm^{-2}, which results from a destructive interference between the $^3S_1$-$^1S_0$ and the $^3D_1$-$^1S_0$ amplitudes. Non-nucleonic degrees of freedom are essential for the interpretation of the data. In a large momentum transfer range, between 10 and 15 fm^{-2}, they account for nearly 100% of the experimental cross section. This process provides some of the most striking evidence of the presence of meson exchange currents in nuclei.

The experimental data are well described by theoretical predictions that allow for π, ρ, and Δ meson exchange currents. Up to ~ 15 fm^{-2} there is almost no sensitivity to the choice of the nucleon-nucleon potential or the πNN form factor. The theoretical predictions for higher momentum transfers strongly depend on the detailed structure of the currents and wave functions.

In order to achieve the best description of the data beyond 10 fm^{-2}, one must include the effects of the π, ρ, and the Δ meson exchange currents

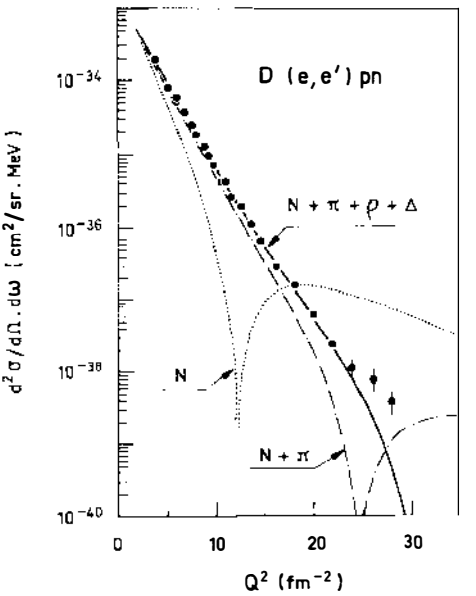

Figure 3 Cross section for threshold electrodisintegration of deuterium at $\theta = 155°$ (13). The impulse approximation result (nucleon current only) (*dotted curve*) with the successive addition of pion exchange (*dot-dash*) and ρ meson and isobar contributions (*solid curve*) are shown (15).

with hadronic form factors at the meson-nucleon vertex. The Dirac form factor F_1 must be used to fit the deuteron electrodisintegration data. The choice of the Sachs form factor G_E would lead to a large discrepancy with experiment. The finite size of the meson-nucleon coupling plays an important role at the spatial scale probed by high momentum transfers. This size is accounted for by a hadronic form factor at the meson-nucleon vertex, with a cutoff parameter $\sim$1200 MeV in the πNN form factor. This corresponds to a size of 0.5 fm for the hadronic interaction region. This value, which is smaller than the proton charge radius, appears to be consistent with the description of the nucleon in a two-phase model where charge and baryon number are fractioned between a quark core and a pion cloud (16). A radius of 0.54 fm is predicted for the core, while the radius of the cloud that includes the ρ meson propagation is 0.91 fm. The difference between the electromagnetic and the hadronic form factors comes from the difference in the coupling of the photon and the pion to the nucleon. The photon, because of its large coupling to the ρ meson, is sensitive to the cloud, while the pion is partially blind to the cloud and probes essentially the size of the nucleon core.

In order to avoid the use of phenomenological hadronic form factors, a different approach was recently proposed (17) in which meson exchange currents are derived from the nucleon-nucleon potential through the continuity equation. The advantage of this procedure is that hadronic form factors are automatically consistent with the nucleon-nucleon potential. This procedure yields results very similar to those of the perturbative approach. Therefore one is quite confident of the reliability of the mesonic description of the electrodisintegration of the deuteron at threshold.

The ρ meson exchange and the Δ isobar current tend to cancel the effect of the πNN form factor. Short-range processes tend to cancel each other in this isovector process, and it seems that the only really significant contribution is due to the π exchange current between two nucleons in a pointlike coupling (18). It is quite intriguing that meson exchange processes appear to be governed by chiral symmetry even at such large momentum transfer. This result suggests that chiral symmetry plays an important role for the description of meson exchange currents beyond the description of soft pions.

A few calculations have begun to investigate the role of quarks with phenomenological models. In the momentum transfer range measured at present, the role of mesons still predominates, quarks making essentially a negligible contribution (19, 20). Experimental data must now be extended to high momentum transfers to investigate such short-range processes.

The most surprising result of this experiment is that there is not yet any sign of breakdown of mesonic theory, even at 1 GeV/c^2, beyond its expected limit of validity.

3.3 *The Magnetic Form Factor of the Deuteron*

The magnetic form factor $B(Q^2)$ of the deuteron is of isoscalar nature. Therefore, the contribution of the pion exchange current derived from chiral symmetry, which plays a central role in isovector processes, vanishes. Thus, one has a unique opportunity to study the effects of other meson exchange currents. Recent experiments (21–23) have considerably extended the momentum transfer range of the measurements of $B(Q^2)$, providing a very discriminating test of theoretical calculations (Figure 4).

Gari & Hyuga (24) have shown that the $\rho\pi\gamma$ exchange current, which is the dominant isoscalar meson exchange current, increases the impulse approximation cross section by a factor of 3 at 30 fm^{-2}, in agreement with experiment. However, beyond 30 fm^{-2}, a smooth falloff is predicted, while the experimental data show a minimum around 50 fm^{-2}.

The effects of $\Delta\Delta$ and NN* (1440) components in the ground state of the deuteron have been investigated with a coupled-channel N-N interaction by Sitarski, Blunden & Lomon (25). They used N-N scattering data

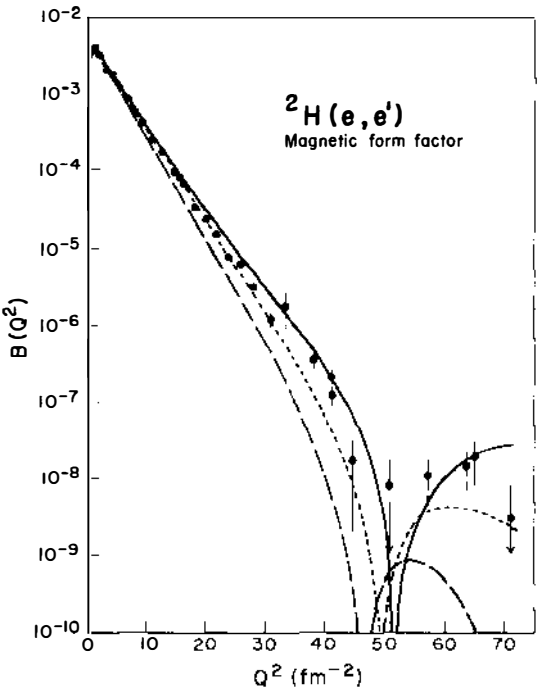

Figure 4 The magnetic form factor of the deuteron $B(Q^2)$. Result from an impulse approximation calculation (*dashed curve*) and the improvement resulting from the inclusion of meson exchange currents and isobar contributions (*dotted curve*) are also shown (25). The solid curve is the result of the Skyrme model (31).

up to 1 GeV, with the magnetic moment and the magnetic form factor of the deuteron as constraints. The form factors of Hoehler et al (26) have been used for the nucleon. The effects of meson exchange, as calculated by Gari & Hyuga (24), have also been included since they are assumed to be relatively independent of the details of the NN potential. This model predicts the existence of a diffraction minimum around 45 fm^{-2}. The best agreement with experiment up to 60 fm^{-2} is obtained with NN(D state) = 5.45%, $\Delta\Delta \approx 1\%$ and $NN^* \approx 0\%$.

Meson exchange currents are of relativistic order for an isoscalar process. The data have reached very high momentum transfers, and a nonrelativistic framework may no longer be reliable for such a light system as the deuteron. At present, it is not yet possible to draw a reliable conclusion on relativistic effects. Various relativistic approaches (27, 28) give completely different predictions. It is crucial to investigate the origin of their discrepancies and to find the appropriate relativistic framework for the description of the properties of the deuteron.

The parton model does not predict a diffraction minimum (29). The existence of a minimum around 50 fm^{-2} shows that even at such high momentum transfers asymptotic behavior has not been reached. Hybrid models (19, 30) involving both nuclear and quark degrees of freedom are able to give a qualitative description of these data.

Nyman & Riska (31) have studied the isoscalar electromagnetic current operator in the Skyrme model. They have shown that this current is determined by the part of the effective QCD Lagrangian that accounts for chiral anomalies and therefore can be predicted at low energies in an essentially model-independent way. The isoscalar meson exchange currents are uniquely related to the baryonic current. It is then possible to derive the form factors of the deuteron from the isoscalar electric structure of the nucleons themselves. This approach gives a good description of the experimental data (see Figure 4).

3.4 *The Trinucleon Systems*

The simplicity of the deuteron makes it a natural starting point for the study of nucleon interactions in nuclei. The success of the impulse approximation, corrected for meson exchange currents, in describing its properties naturally leads one to ask whether this scheme can be as successful for more complex nuclei. In such systems short-range interactions play a different role; the deuteron is barely bound (1 MeV/nucleon instead of the 8 MeV/nucleon typical of heavy nuclei) and the two nucleons rarely find themselves at close proximity. Moreover, the influence of many-body forces (3-body forces in particular) or isospin-dependent effects cannot be examined (32). These aspects of the nuclear force can be studied in the trinucleon systems (^{3}He and ^{3}H).

The calculation of properties of $A = 3$ nuclei with realistic forces is now reliable: Hamiltonians based on realistic two-body interactions yield almost identical results (33, 34) for the binding energies of ^{3}He and ^{3}H, results that are significantly lower than the experimental values (7.72 and 8.49 MeV). The difference between experiment and theory for the binding energy of the $A = 3$ system is now believed to arise largely from the three-nucleon force (33). Only the long-range (attractive) part of the three-body force, which is attributed to two-pion exchange, is well understood. The short-range part is believed to be repulsive and is adjusted phenomenologically. In a more ambitious approach (35) both the short- and long-range parts of the three-body force are derived microscopically by including meson exchange and isobar degrees of freedom. These calculations render support to the phenomenological approach by producing similar trends. The effect of the three-body force is to increase the binding energy by 1–3% of its potential energy. The resulting smaller root mean square (rms) radii are also in agreement with the experimental values. The detailed study of the charge and magnetic form factors of ^{3}H and ^{3}He can provide further insights on the structure and the momentum content of the ground state.

3.5 *The Form Factors of ^{3}H and ^{3}He*

Elastic electron scattering cross section from ^{3}H or ^{3}He is a linear combination of the squares of the charge and magnetic form factors. Recent measurements (36, 42) separated both form factors up to ~ 25 fm^{-2}. Figure 5 provides a comparison of the experimental data for the charge form factors to the theoretical predictions of Hajduk et al (35). The impulse approximation, which accounts only for nucleon currents, does not describe the data correctly. The diffraction minimum is shifted by 3 fm^{-2}, while the amplitude of the calculated second diffraction maximum is too low by a factor of 2. Various combinations of two-body and three-body forces have been investigated (33, 37). None of them is able to account for the experimental charge form factors. The influence of the three-body force on their shape is very small. A larger negative contribution that vanishes at $q = 0$ and that increases up to the second diffraction maximum is needed. There is a term in the two-pion exchange three-nucleon interaction that gives such a contribution, but in order to explain the observed form factors its strength has to be increased beyond reasonable limits (37).

As in the case of the deuteron, the charge form factors of the three-nucleon system cannot be described without the explicit introduction of nonnucleonic degrees of freedom. A reasonable agreement is obtained for the charge form factors of ^{3}He and ^{3}H when the effects of Δ isobars and meson exchange currents are included (35, 38) (see Figure 5).

In a nonrelativistic framework, the relative importance of the meson

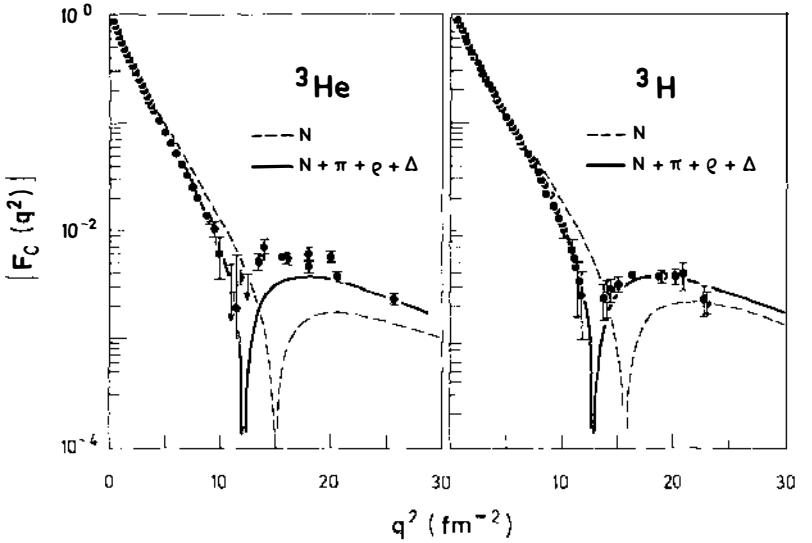

Figure 5 The charge form factors of ^{3}H and ^{3}He. The dashed curve depicts the impulse approximation results. The solid curve derives from a calculation in which meson exchange contributions are included (35).

exchange currents depends on the choice of the pion-nucleon coupling. In the pseudoscalar coupling the isoscalar and the isovector meson exchange contributions have approximately the same magnitude. In ^{3}He the two contributions have the same sign, so the ^{3}He form factor is not very sensitive to the choice of coupling. In ^{3}H and for pseudoscalar coupling they contribute with opposite signs, which leads to an almost complete cancellation. Such a cancellation is not observed experimentally.

A description of the same data has also been attempted with quark models (39, 40). Results similar to those of traditional models employing pseudovector coupling are obtained. The photon is coupled to a quark-antiquark pair instead of the usual nucleon-antinucleon pair used for the pion exchange current. The ^{3}He form factor has been also described with quark cluster models (40). These calculations are in reasonable agreement with experiment but have a large model dependence.

The major sources of uncertainty in the theoretical description of the trinucleon charge form factors are of relativistic origin (41). Meson exchange currents are relativistic corrections, while the three-body wave functions are calculated in a nonrelativistic framework. Unfortunately, at this point we lack the appropriate theoretical framework for incorporating in a consistent and complete fashion relativistic corrections.

The magnetic form factors of ^{3}H and ^{3}He (42) are shown in Figure 6. They correspond to an M1 isovector transition similar to the elec-

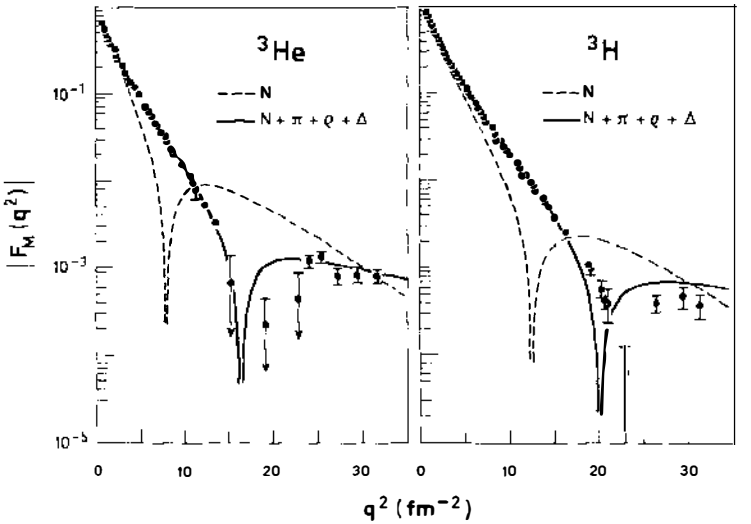

Figure 6 The magnetic form factors of ^{3}He and ^{3}He. The curves are defined as in Figure 5.

trodisintegration of the deuteron. The impulse approximation alone cannot explain the experimental data. In the region of $q^2 = 8$ fm^{-2} for ^{3}He and 12 fm^{-2} for ^{3}H, the cross section is entirely due to nonnucleonic processes because of destructive interference among the nucleonic amplitudes. The prediction of Strueve, Hajduk & Sauer (43), which takes into account the effect of both π and ρ meson exchange currents, agrees with the experimental data up to the diffraction minimum. In the region of the second diffraction maximum, there is a slight deviation from experiment. The calculation of Hadjimichael, Goulard & Bornais (38) is also in good agreement with the ^{3}He and ^{3}H magnetic form factors. Similar calculations have been performed by Riska (44) and by Maize & Kim (45). In the expression of the exchange current operators, one must use the Dirac form factor F1 to reproduce the experimental data, while there is strong discrepancy at large momentum transfers when the Sachs form factor G_E is used. As in the case of deuteron electrodisintegration (18), the magnetic form factor of ^{3}He can be well described by the impulse approximation corrected only by the contribution of soft pions. This result further highlights the significance of chiral symmetry.

Experiment and theory have made major advances in the three-nucleon problem. The two-body contribution is now theoretically well under control and thus enables us to establish the presence of nonnucleonic processes. Remaining uncertainties are at the level of relativistic effects and of the short-range part of the three-body force.

4. ELASTIC ELECTRON SCATTERING FROM HEAVY NUCLEI

The simplicity of few-nucleon systems is ideal for a detailed study of nucleon-nucleon interactions in a nucleus. However, these very light nuclei do not exhibit the special characteristic features of nuclear matter, such as saturation of the nuclear force and a constant binding energy per nucleon. In addition, collective behavior (an important degree of freedom in many-body systems) is totally absent. Such features can only be studied in heavy nuclei. There one is faced with the additional problem of isolating the properties of the bulk nuclear matter from those of the nuclear surface. Nuclear matter is the only form of matter that cannot be studied experimentally in bulk. Nuclear physicists are faced with the challenge of having to derive bulk properties from the behavior of droplets of nuclear matter, the atomic nuclei. The superb spatial resolution and penetrability of electron scattering facilitates the study of the interior of heavy nuclei, thus enabling the isolation of bulk properties from surface effects.

4.1 *Charge Distributions of Magic Nuclei*

The charge distribution of nuclei can be determined from the elastic electron scattering cross section. As late as 1975 the interior charge densities of medium and heavy nuclei had not been determined with sufficient accuracy to provide stringent tests for the emerging Hartree-Fock calculations (46). New electron scattering data, combined with the very precise measurements of muonic x-ray transitions, have since then determined the charge densities in the interior of many nuclei to an accuracy of 1%. This set of data, which is the culmination of an experimental effort spanning 35 years, offers a remarkably precise and well-understood nuclear structure observable. Typical is the case of ^{208}Pb (see Figure 7), where the elastic cross section has been measured over 13 orders of magnitude (47). Presently no nuclear model can reproduce the cross section to the experimental accuracy. The observed discrepancies have provided a crucial impetus for the advancement of nuclear many-body theory.

The experimental charge densities for all doubly closed-shell nuclei (47–52; D. Goutte, private communication) are compared in Figure 8 with the prediction of a mean field (Hartree-Fock-Bogoliubov, HFB) calculation by Dechargé & Gogny (53) with a finite-range, density-dependent, effective force. The disagreement is most pronounced in ^{208}Pb, which a priori seemed the most favorable case for a mean field description. In the mean field approach the interactions of a nucleon with all the other nucleons is approximated by an effective potential. This comparison shows that modern mean field calculations with effective interactions rather accu-

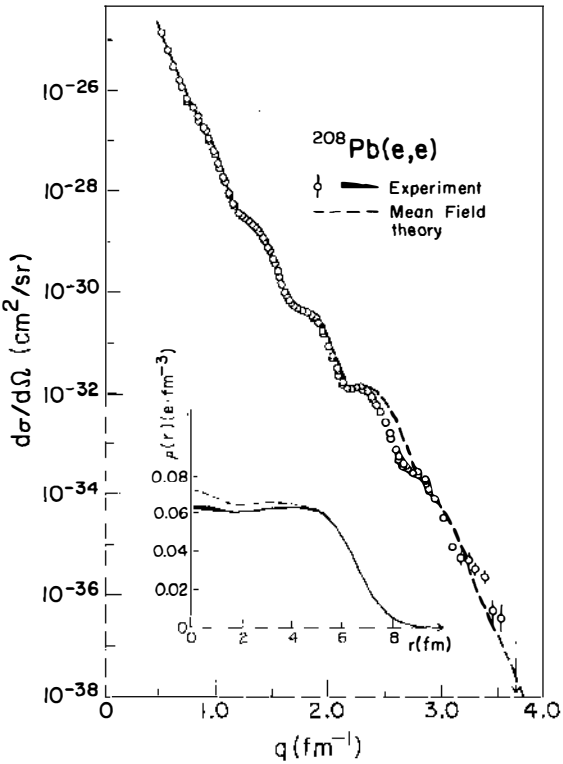

Figure 7 Elastic cross section from ^{208}Pb (47). The dynamic range of the measurements allows the reconstruction of the charge density distribution (*insert*). The thickness of the line in $\rho(r)$ depicts the experimental uncertainty. The mean field result in that of Dechargé & Gogny (53).

rately describe sizes and surface properties but systematically predict larger charge density fluctuations in the nuclear interior.

This discrepancy is today understood as arising largely from correlations whose effects cannot be incorporated into the mean field approach to the nuclear many-body problem. The effects of short-range correlations on the single-particle wave functions are partly accounted for by the introduction of density dependence in the effective nucleon-nucleon potential. The Pauli principle tends to diminish their significance since nucleons cannot scatter into occupied states, which explains why mean field theory is successful in dense systems such as nuclei. However, the effect of long-range correlations due to collective excitations such as the low-lying collective states and the giant resonances are not taken into account. Such correlations are most reliable when calculated consistently with the same force used to generate the Hartree-Fock (HF) ground state (54). They

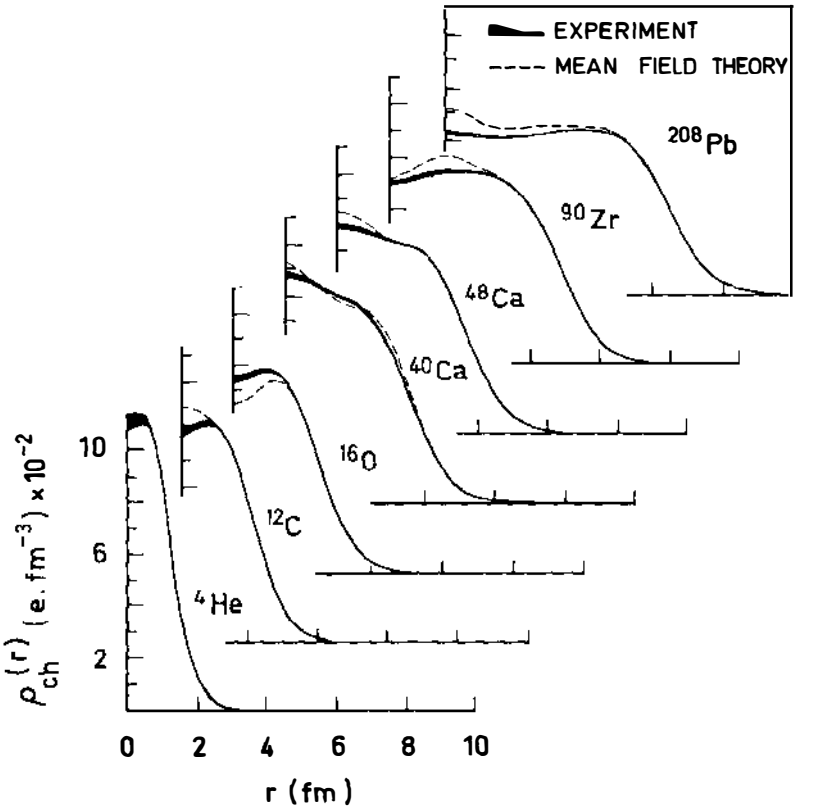

Figure 8 Charge density distributions of doubly closed-shell nuclei. The thickness of the solid line depicts the experimental uncertainty. The mean field calculations are from (53).

have been estimated in the framework of the random phase approximation (RPA) (55), which is equivalent to time-dependent Hartree-Fock in the limit of small amplitudes. The large interior fluctuations predicted by mean field theory are damped by the RPA correlations. However, such corrections are not sufficient to reconcile theory and experiment.

It is then important to test whether the RPA provides a reasonable description of the collective excitations of magic nuclei. The measured transition charge densities (56, 58, 60; K. Seth, private communication; J. Heisenberg, private communication) for the lowest octupole (3^-) vibrations in magic nuclei are compared to RPA predictions (61) in Figure 9. These states are highly collective, exhausting a substantial fraction of the energy-weighted sum rule (EWSR) (typically 30%). Most of the transition charge is found concentrated in the surface. In light nuclei such

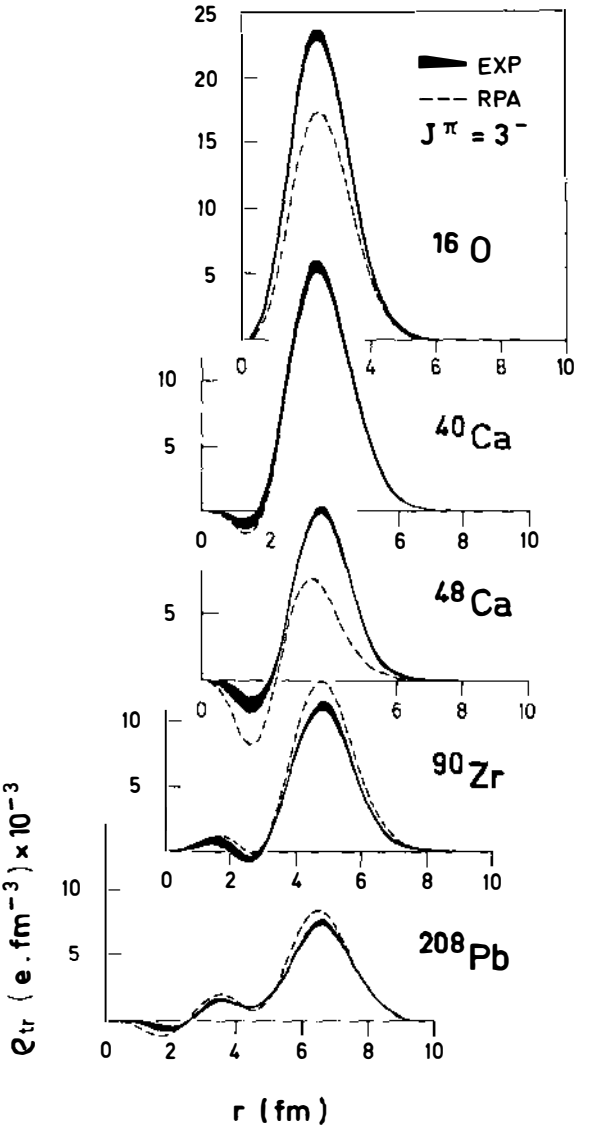

Figure 9 Transition charge densities for the first collective octupole vibrations of doubly closed-shell nuclei (56, 58, 60; K. Seth, private communication; J. Heisenberg, private communication). Same conventions as Figure 8. The theoretical predictions (53–55; Dechargé & Gogny, private communication) are obtained in a self-consistent RPA calculation.

as ^{16}O, the absence of interior structure is striking. It is only in heavy nuclei, ^{90}Zr and ^{208}Pb, that fluctuations in the interior are observed. RPA indeed provides a reasonable overall description of collective excitations—at least at low excitation energies. In RPA, as in HF, the theoretical fluctuations are too large in the nuclear interior, which indicates a systematic problem of a more fundamental nature.

The inability of mean field theory to describe accurately the ground-state charge densities and the octupole transition charge densities of magic nuclei in the nuclear interior raises a fundamental question: "To what extent can a correlated wave function be approximated by an independent particle wave function?" A definitive answer has been obtained by isolating the charge distribution of a 3s proton and by studying single-particle distributions in the lead region.

4.2 *Single-Particle Distributions*

In the independent particle description, the charge distribution is simply the sum of the squares of the proton wave functions in the ground state. The narrow structure in the center of ^{208}Pb is attributed to the two 3s protons occupying the valence orbit. The quenching of this structure in the measured charge density indicates that the 3s density distribution is significantly modified. Correlations could deform the radial structure of the 3s wave function or modify its occupation probability.

The detailed study of the interior of the charge distributions of ^{206}Pb and ^{205}Tl offers the possibility of learning about the shape and strength of the proton 3s orbital. Figure 10 shows the variation of the ratio of the cross sections of ^{205}Tl to ^{206}Pb (62, 63) as a function of the momentum transferred to the nucleus. The very special shape of the 3s orbit produces a narrow structure at high momentum transfer and thus allows the unambiguous identification of the contribution of the 3s proton. Mean field theory, regardless of the detailed assumptions of various models, correctly predicts a peak of large amplitude, totally different from the usual small fluctuations between neighboring nuclei. The phase and the shape of the calculated oscillations are in remarkable agreement with the experimental result, but an almost uniform reduction of 30 to 35% in their amplitude is observed. This peak, in the ratio of cross sections of ^{205}Tl to ^{206}Pb, is the signature of the shell model.

Figure 11 shows the charge difference between ^{206}Pb and ^{205}Tl (63, 64). The characteristic shape of the 3s orbit is observed. Experiment and theory also have the same remarkable similarity in configuration space as in momentum space. It is the first time that the spatial distribution of a particle in a quantum orbit has been isolated. The concept of an independent particle orbit has thus been demonstrated to be valid in the nuclear interior.

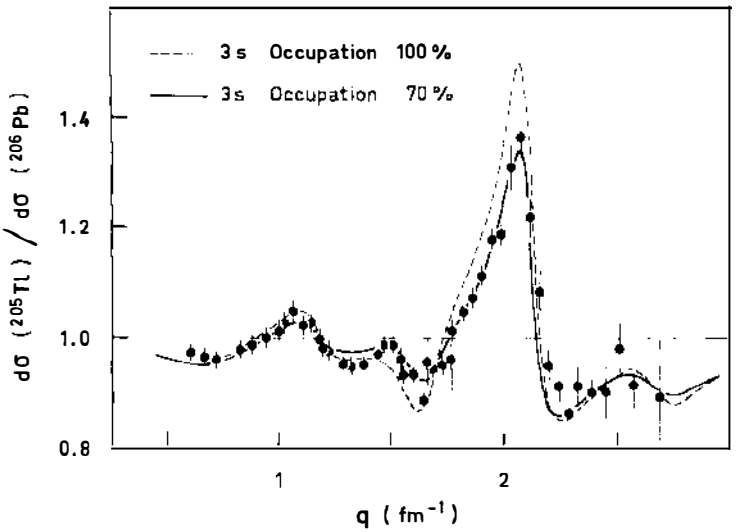

Figure 10 The ratio of elastic cross sections from ^{205}Tl and ^{206}Pb (62, 63). The peak at $q = 2$ fm^{-1} is the signature of the 3s orbit. The curves are mean field predictions due to X. Campi.

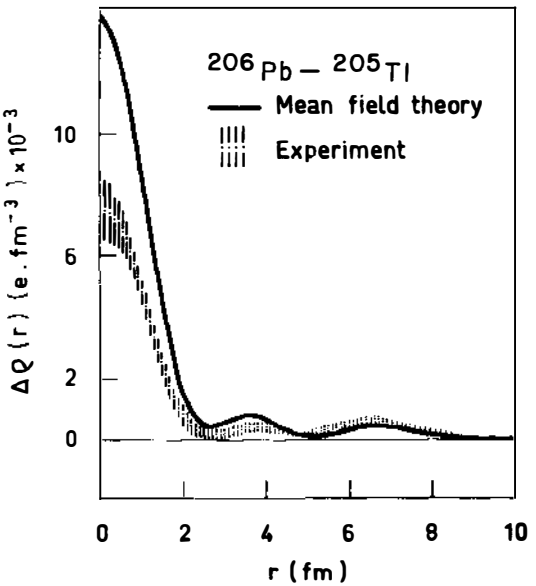

Figure 11 The charge density difference of ^{206}Pb and ^{205}Tl (63, 64).

One observes clearly a uniform reduction of the charge difference in the interior of the nucleus for $0 \leq r \leq 5$ fm. The fraction of charge that has left the center of the nucleus is redistributed at its surface.

Significant information on single-particle distributions and the limits of the mean field description is also provided by elastic magnetic scattering (1).

The measured form factor of ^{207}Pb is shown in Figure 12. The orbital responsible for the magnetization density of ^{207}Pb is the unpaired $3p_{1/2}$ neutron; its quantum number allows a single M1 multipole with high concentration of magnetization density at the center of the nucleus. The low frequency limit of this measurement is the magnetic moment of ^{207}Pb, which agrees rather well with the Schmidt value. This agreement historically has been presented as one of the triumphs of the shell model. Electron scattering shows that, in fact, the modification of the ^{207}Pb magnetization distribution due to correlations is substantial. A quenching of 0.7 ± 0.1 of the single-particle amplitude is observed at high momentum transfers.

The form factor of ^{205}Tl arising from the unpaired $3s_{1/2}$ proton is quenched even further than that of ^{207}Pb. This is due to the configuration mixing resulting from coupling to the low-lying 2^+ states of ^{206}Pb. When this configuration mixing is accounted for, a quenching identical to that of ^{207}Pb is obtained at high momentum transfers ($q \approx 2.3$ fm^{-1}) (65). The same quenching factor (0.7 ± 0.1) is also found for the magnetic form factor of ^{209}Bi (66).

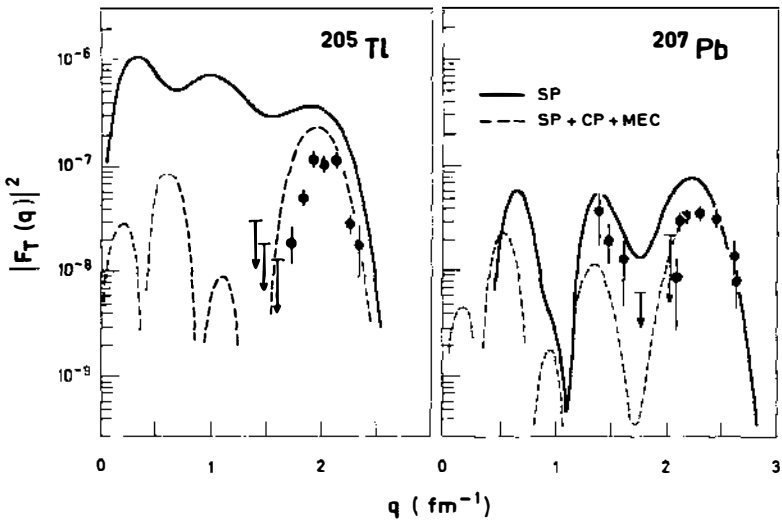

Figure 12 The elastic magnetic form factors of ^{207}Pb and ^{205}Tl (65). The solid curve depicts the single-particle predictions (53). The dashed curve includes in addition the effects of core polarization and meson exchange (67, 68).

The most complete available calculation in the mean field approach is that of Suzuki et al (67, 68), in which the effects of first-order core polarization, π and ρ exchange, and Δ-h excitations have been explicitly accounted for. This calculation predicts the very strong modification of the form factor of ^{205}Tl at intermediate q, which is attributed to first-order tensor core polarization (Figure 12).

The elastic magnetic scattering from ^{205}Tl, ^{207}Pb, and ^{209}Bi, like all single-particle transitions studied by elastic or inelastic electron scattering in the Pb region, exhibits a systematic reduction from the mean field result regardless of the multipolarity or the character of the transition (3, 69). This reduction in the case of the lead region is of the order of 0.7 and was attributed to the effect of correlations that significantly modify the occupation probabilities. In this approach the quenching at high momentum transfer of the magnetization form factors of ^{205}Tl, ^{207}Pb, and ^{209}Bi measures directly the discontinuity of occupation probabilities immediately below (n_-) and above (n_+) the Fermi sea. The deduced Z factor ($Z = n_- - n_+$) for both neutron and proton shells is $Q = 0.7 \pm 0.07$. Mean field theory by definition produces $Z = 1$. An estimate (69) of the occupation numbers, shown in Figure 13, in ^{208}Pb is obtained by adding to the microscopically calculated nuclear matter occupation numbers (70) the effects of RPA correlations (55). The resulting quenching factors are in agreement with the experimental results. Similar conclusions have been reached by Mahaux and coworkers (71) by examining the enhancement of the effective mass of nucleons at the Fermi energy.

Making (c, e'p) measurements on ^{206,208}Pb and ^{205}Tl provides comple-

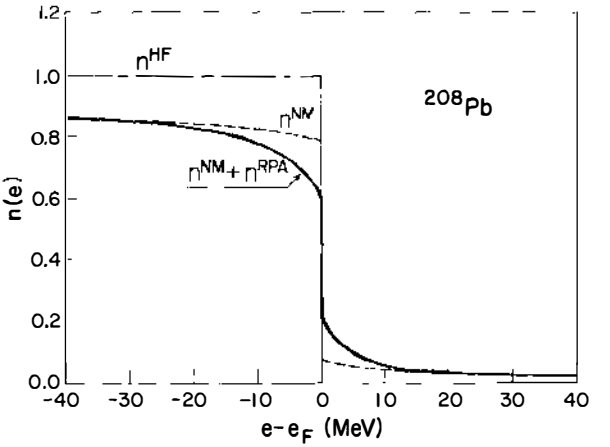

Figure 13 An estimate of occupation numbers in ^{208}Pb (*thick line*) derived from a nuclear matter calculation to which the effects of RPA correlations have been added (69).

mentary information on the momentum distribution of orbits as well as on their spectroscopic factors. The missing mass resolution of 100 keV achieved recently at NIKHEF-K (72) is a technological breakthrough that has made these experiments possible. An occupation probability of 0.8 ± 0.1 is derived for the $3s_{1/2}$ orbit of ^{208}Pb, which confirms the interpretation of the elastic scattering measurements discussed earlier. Jaminon et al (73) have stressed that in a mean field approach it is not possible to reproduce simultaneously the charge and the momentum distribution. Additional information is then expected to emerge from the determination measurements of the momentum distribution of heavy nuclei through (e, e′p) measurements, especially at high momenta where the effect of correlations is predicted to be important.

4.3 *Coupling of Single-Particle to Collective Modes*

The interplay between single-particle and collective degrees of freedom not only is one of the most interesting consequences of collective behavior, it also allows the extraction of bulk properties through the study of single-particle properties. Recent precise measurements spanning a large dynamic range in momentum transfer have allowed us to test our theoretical understanding of such processes and to gain access to bulk properties such as the compressibility of nuclear matter.

The determination of the charge differences between ^{208}Pb, ^{207}Pb, ^{206}Pb, and ^{204}Pb from a combined analysis of muonic x-ray and electron scattering data measures the rearrangement of charge that results from the successive removal of neutrons from the doubly closed shell of ^{208}Pb.

Mean field theory (53, 61) describes the isotopic density differences well. Excellent agreement is achieved despite the fact that the same theory does not successfully describe the charge distribution of each individual isotope. The isotopic density differences in the Pb region are mostly sensitive to three effects: the nuclear compressibility, the neutron pairing, and the electromagnetic spin-orbit contribution. In the case of the ^{207}Pb-^{208}Pb difference, pairing plays no role at all; ^{207}Pb is described by a neutron hole in ^{208}Pb. Since the electromagnetic spin-orbit effect can be calculated reliably, quantitative information on the nuclear compressibility can be deduced from the ^{207}Pb-^{208}Pb difference. Figure 14 shows a comparison between the experimentally derived density difference (74) and the results of two HFB calculations performed with two versions of Gogny's D1 force (53). These forces differ in their values of compressibility formula ($\kappa =$ 228 MeV, $\kappa = 209$ MeV) but otherwise provide equally good fits to the set of observables used to adjust the force parameters. The data show a clear preference for $\kappa = 230$ MeV. This value of κ is in agreement with the values derived from the analysis of breathing mode energies.

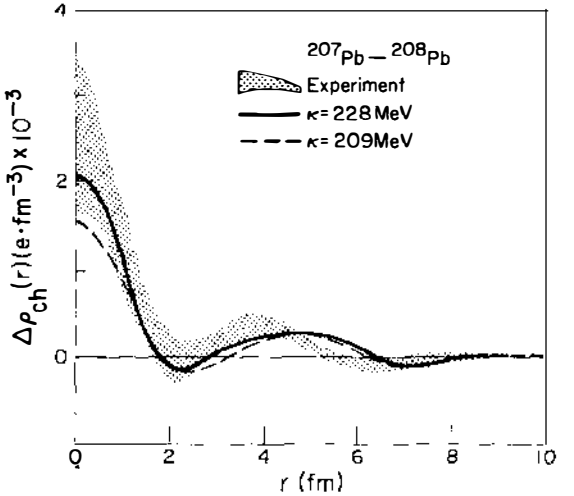

Figure 14 Experimental ^{207}Pb-^{208}Pb charge density difference together with mean field predictions for two values of the nuclear compressibility (74).

5. ELECTRON-NUCLEON SCATTERING IN THE NUCLEAR MEDIUM

Electron scattering from nuclei at energy transfers large compared to nucleon separation energies is dominated by interactions with quasifree nucleons. Recent inclusive measurements have studied quasielastic scattering and the excitation of the Δ isobar in a variety of nuclei.

5.1 *Quasielastic Scattering*

A prominent feature of the spectrum of inelastically scattered electrons by the nucleus is the result of quasielastic scattering (see Figure 1). It manifests itself as a broad peak at $\omega \approx (q^2/2m)+\bar{\varepsilon}$, where $\bar{\varepsilon}$ is the average binding energy per nucleon and m its effective mass.

The simplest description of this process is given in terms of the noninteracting Fermi gas model, in which the nucleons are confined within the nuclear volume occupying levels up to Fermi momentum k_F. In this model, the experimentally observed quasielastic peak is viewed as providing direct information on $\bar{\varepsilon}$ and k_F. The position of the quasielastic peak determines $\bar{\varepsilon}$, while its width determines k_F. Earlier measurements (75) showed an excellent agreement with this simple picture. The shape of the quasielastic cross section was found by Moniz et al (76) to be very well described by a two-parameter fit. The values k_F and $\bar{\varepsilon}$, derived for a variety of nuclei, were found in reasonable agreement with the widely accepted values.

More realistic shell-model calculations provided further credence to the noninteracting Fermi gas model by reproducing its results. In these calculations, the average binding energy $\bar{\varepsilon}$ is determined by a microscopic calculation, and final-state interactions are calculated by assuming that the ejected nucleon moves in the potential of the residual nucleus (77). The excellent agreement between experiment and theory suggested that there should not be any difficulty in describing separately the longitudinal and the transverse response functions. Furthermore these first measurements were interpreted as indicating that quasielastic electron scattering was well understood in the framework of the independent particle model.

5.2 *Longitudinal and Transverse Response Functions*

The agreement between the independent particle model and the inclusive quasielastic electron scattering cross section turned out to be completely fortuitous. The same model failed to account for the separated longitudinal and transverse response functions $R_L(q,\omega)$ and $R_T(q,\omega)$ for a variety of nuclei (78–83). Figure 15 shows the longitudinal and transverse response functions for ^{40}Ca at a momentum transfer of 410 MeV/c. The parameters of the Fermi gas model $k_F = 250$ MeV/c and $\bar{\varepsilon} = 36$ MeV were taken from a fit that successfully describes the unseparated cross section. The measured $R_L(q,\omega)$ shows significantly less strength at the peak as compared to the theoretical prediction.

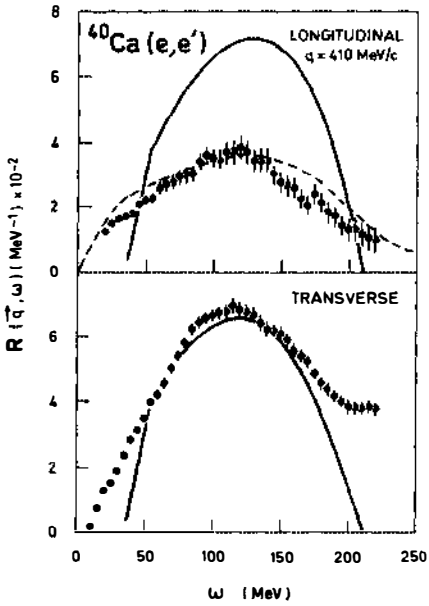

Figure 15 ^{40}Ca longitudinal and transverse response functions at $q = 410$ MeV/c (81). The solid curve is the Fermi gas prediction. The dashed curve is the result of a calculation for nuclear matter that treats correlations (97).

It was generally expected that the transverse response function would not be reproduced by calculations that neglect nonnucleonic degrees of freedom. Since meson exchange currents and delta isobar excitations are predominantly transverse, it turns out that its shape, up to $q = 400$ MeV/c, is not very sensitive to theoretical hypotheses and is reasonably well explained by nearly all standard calculations. Only at higher momentum transfers, $q = 550$ MeV/c, is a significant effect of nonnucleonic components found.

Similar results are observed for a variety of nuclei. In the momentum transfer range between 200 and 600 MeV/c, predictions based on the independent particle model are unable to account for the shape and the strength of the longitudinal response function. At present no theoretical model is able to describe simultaneously the longitudinal and the transverse response functions of nuclei heavier than ^{12}C. The situation is different for ^{3}He, for which both the longitudinal and the transverse response functions are well described by theory.

5.3 *The Longitudinal Sum Rule*

The longitudinal structure function $S_L(q)$ is defined in terms of the longitudinal response by the integral

$$S_L(q) = \frac{1}{Z}\int_{\text{inel}} \frac{R_L(q,\omega)\,d\omega}{|\tilde{G}_E(q_\mu^2)|^2}, \qquad 6.$$

where Z is the charge of the target nucleus and $\tilde{G}_E$ is the appropriate free nucleon form factor (84). By integrating over all excitation energies of the nucleus, the following identity is obtained (84a, 85):

$$S_L(q) = 1 + \frac{1}{Z}\int_0^\infty e^{-iq(r_1-r_2)} C_2(\mathbf{r}_1, \mathbf{r}_2)\,d\mathbf{r}_1\,d\mathbf{r}_2, \qquad 7.$$

where $C_2(\mathbf{r}_1, \mathbf{r}_2)$ is the two-body correlation function defined in terms of one- and two-body densities:

$$C_2(\mathbf{r}_1, \mathbf{r}_2) = \rho_2(\mathbf{r}_1, \mathbf{r}_2) - \rho_1(\mathbf{r}_1)\rho_1(\mathbf{r}_2). \qquad 8.$$

Ignoring relativistic corrections, conservation of electric charge requires that $S_L(q) \to 1$ for $q \to \infty$, where the contribution of correlation vanishes.

The asymptotic limit is generally assumed to be reached for $q > 2k_F$ when the effect of two-nucleon correlations is expected to be negligible. Figure 16 shows the behavior of $S_L(q)$ for ^{3}He and ^{40}Ca as a function of q, between 200 and 600 MeV/c. The experimental data are compared to the calculation of Schiavilla et al (85). While the asymptotic value is reached for ^{3}He at $q = 500$ MeV/c, 40% of the sum rule is still missing for ^{40}Ca and all heavier nuclei with the possible exception of ^{238}U (83).

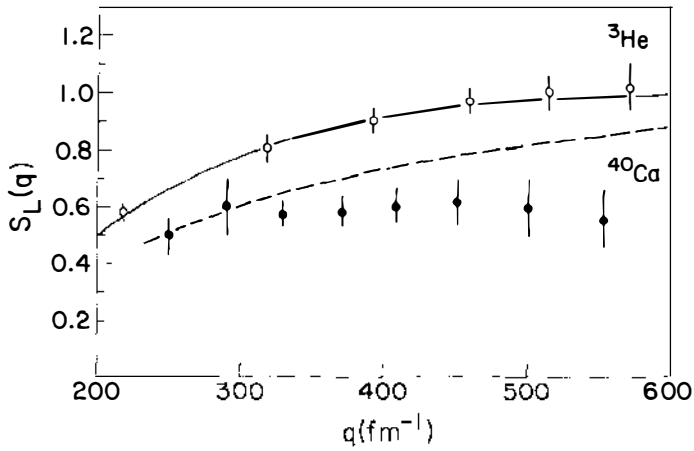

Figure 16 The Coulomb sum rule for quasielastic scattering from ^{3}He and ^{40}Ca. The solid curve results from an exact three-body calculation for ^{3}He (85). The dashed curve derives from the same nuclear matter calculation (97) whose results are shown in Figure 15.

5.4 *The Missing Longitudinal Strength*

The discrepancy between theory and experiment has stimulated an intense theoretical activity. The prescription for the off-shell nucleon current operator is sufficiently well constrained by Lorentz and gauge invariance to be a negligible source of uncertainty (84). Different mechanisms have been invoked to explain the missing longitudinal strength; most notably relativistic effects, modification of the nucleon properties in the nuclear medium, and many-body correlations.

Relativistic effects have been investigated in some detail (86) in the mean field theoretical framework based on Dirac phenomenology. Calculations have been performed in the framework of the σ-ω model developed by Walecka and coworkers (87). The discrepancy between experiment and results from relativistic models is smaller than in their nonrelativistic counterparts. This is because the effective nucleon mass and the energy scale are modified by the presence of scalar σ and vector ω fields, $m \rightarrow m^* = m + V_s$ and $E \rightarrow E^* = E - V_0$, with typical values $V_s = -400$ MeV and $V_0 = +300$ MeV for the scalar and vector potentials. The resulting effective mass m^* enters differently in the charge and current operators. However, recent calculations (88) have shown that such relativistic effects may play a role, but they are not sufficient to explain quasielastic electron scattering data.

The hypothesis of a significant modification of the properties of the nucleon in the nuclear medium has received much attention. An increase

of the nucleon radius (confinement volume) would quench both the longitudinal and transverse response functions. An increase of $\sim 20\%$ of the nucleon size reconciles theory and experiment for ^{56}Fe (89). It also provides a possible explanation of the EMC effect. Celenza et al (90) have developed a model that predicts such an increase. This model is an attempt to make the synthesis of a soliton bag model for the nucleon and Dirac phenomenology. In addition to the standard quark fields, the σ, ω, π, ρ fields are used to build the soliton. The electromagnetic radii of the free nucleon are reasonably well described by this model. In the nuclear medium, the presence of the other nucleons modifies the σ and ω fields. The size of the nucleon increases as a function of the nuclear density, becoming 20% larger for lead. This model reproduces the longitudinal response function measured experimentally, but its prediction for the transverse response function is not compatible with the experimental result (91).

The behavior of the nucleon form factor in the nuclear medium has been studied (A. Magnon, private communication) via the ^{40}Ca(e, e′p) reaction for momentum transfers between 300 and 800 MeV/c. As in the inclusive process, the ratio of the longitudinal and transverse response functions is quenched by 35% with respect to theory. It has also been found that within experimental uncertainties the momentum transfer dependence of the electron-nucleon cross section in the nuclear medium is compatible to that of the free nucleon. This result disagrees with the predictions of Celenza et al (90). An increase of the nucleon radius larger than a few percent is excluded by this measurement. A similar conclusion was reached from a y-scaling analysis of ^{56}Fe quasielastic data, which is discussed in the following section. A significant swelling of nucleons does not appear to be the explanation of the missing longitudinal strength.

Many-body correlations can be very significant in influencing the longitudinal response function but up until recently their effect at 400 MeV/c was predicted to be small. Correlations due to collective excitations of the nucleus improve the agreement with theory at $q = 300$ MeV/c (93–96), but their effect decreases at higher momentum transfer. At $q = 550$ MeV/c, these long-range correlations calculated in the framework of the random phase approximation become essentially negligible. Short-range and tensor correlations have been difficult to estimate in a reliable way (96, 97) because realistic calculations are possible only for few-nucleon systems and for nuclear matter. Calculations for finite nuclei are usually performed with effective interactions, which predict only a small effect for momentum transfers $q = 400$ MeV/c.

Fantoni, Pandharipande, and coworkers recently showed a large effect due to correlations in calculations performed with realistic nucleon-nucleon interactions in the few-nucleon systems (85) and in nuclear matter

(97). The effect of these correlations is to quench the amplitude of the quasielastic peak and to shift a significant fraction of its strength at higher excitation energies. The longitudinal response calculated for nuclear matter (97) is compared to experimental data for ^{40}Ca at $q = 410$ MeV/c in Figure 15. This theoretical prediction is in good agreement with experiment. The missing longitudinal strength is simply shifted beyond the maximum excitation energy measured experimentally. The longitudinal sum rule for nuclear matter is compared in Figure 16 to the experimental data for ^{40}Ca (81, 82). The upper limit of integration of theoretical response was taken to be identical to the experimental one. Substantially better agreement with experiment is achieved by this calculation than by other theoretical approaches, but there is still some missing strength at high q. At 550 MeV/c, the ^{40}Ca and ^{56}Fe longitudinal response functions are overpredicted for excitation energies exceeding 200 MeV. This might be due to a number of approximations in the calculation. It is also quite possible that the excitation of the nucleon, which is not taken into account, is beginning to play a significant role.

The available data are still relatively limited in momentum transfer. It is important to extend these data to higher q where the discrepancy is most serious. Further calculations with a realistic nucleon-nucleon interaction for finite nuclei are now crucial in order to reach a definitive conclusion on the capabilities and limitations of the traditional approach. The modification of the nucleon properties in the nuclear medium and relativistic effects appears to be less important than many-body correlations in explaining quasielastic electron scattering data.

5.5 *Y-Scaling of the Quasielastic Response Function*

The inclusive (e, e′) cross section in the quasielastic region has a shape and an amplitude that varies smoothly as a function of both the momentum transfer q and the excitation energy ω. In the impulse approximation, assuming a single-photon exchange, the cross section can be written as

$$\frac{d^2\sigma}{d\Omega\, d\omega} = \left(Z\frac{d\sigma_p}{d\Omega} + N\frac{d\sigma_n}{d\Omega} \right) R(q,\omega), \qquad 9.$$

where $d\sigma_p/d\Omega$ and $d\sigma_n/d\Omega$ are the proton and neutron cross sections.

West (98) has shown that if, in addition, one assumes a nonrelativistic Hamiltonian and neglects final-state interactions, then the response function $R(q, \omega)$ can be expressed in terms of a single variable y, for large energy and momentum transfer:

$$R(q,\omega) \to F(y) \qquad \text{for } q \to \infty, \qquad 10.$$

where

$$y \equiv \mathbf{k} \cdot \hat{q}; \qquad y \approx \frac{(\omega^2 + 2M_n\omega - q^2)}{2q}. \tag{11.}$$

After dividing by the electron-nucleon cross section, the experimental data measured for different values of q and ω should lie on a universal curve (98). The scaling variable y defined above is the component of the struck nucleon momentum $\mathbf{k}$ along the momentum transfer $\mathbf{q}$. The choice of y depends on the theoretical assumptions used to describe final-state interactions, but Gurvitz, Tjon & Wallace (99) have shown that y-scaling is observed for a variety of possible y variables.

The cross sections for ^{3}He (see Figure 17) (100) and more recently those for ^{4}He, ^{12}C, ^{27}Al, ^{56}Fe, and ^{197}Au (101) have been measured for a wide range of momentum transfers and excitation energies. The experimental data, when plotted as a function of y, lie on a universal curve in the quasielastic region (Figure 18*a*). The region of the quasielastic peak for which scaling behavior is observed is the region of small y, where $y < 0$. For $y > 0$, the response function does not scale. This can be understood easily, as $y > 0$ corresponds to an energy transfer sufficiently large to excite nucleon resonances that have form factors different from that of the free nucleon.

It is intriguing that at present no calculation based on a purely nucleonic

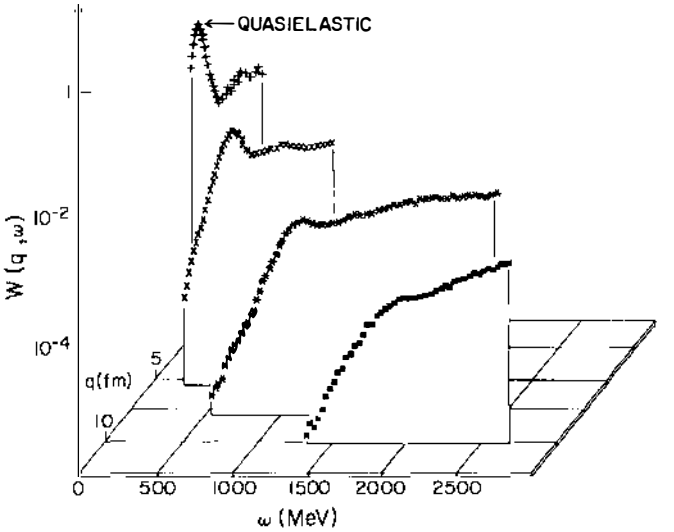

Figure 17 ^{3}He(e, e′) response function in the quasielastic region for four different momentum transfers (101).

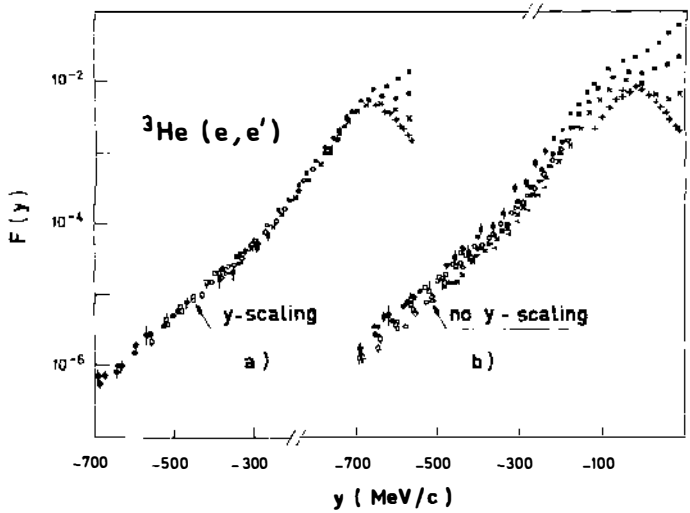

Figure 18 Scaling function $F(y)$ for ^{3}He. The scaled data derive from the nuclear response functions shown in Figure 17 obtained by using (*a*) the free nucleon form factor and (*b*) a modified form factor corresponding to a size increase of the nucleon of 10% and simultaneously a mass decrease of 10% (104).

picture is able to reproduce the asymptotic scaling behavior of the experimental data. The theoretical spectral functions underpredict the data, which indicates a lack of high momentum components or nonasymptotic behavior where the effects of binding are still being felt (101a). Experimental information on the nucleon momentum distribution has been obtained at lower momentum transfers by measuring ^{3}He(e, e′p) cross sections (102). These data are reasonably well reproduced by theoretical calculations (103). Therefore it is crucial to find if the problem lies in the breakdown of the theoretical description of the nucleon momentum distribution at very high momentum, or in the description of the reaction mechanism, as suggested by Ciofi degli Atti et al (99, 101a). The present ^{3}He(e, e′) data have a very small ($<15\%$) longitudinal component. We discussed in the previous section that it is the longitudinal response that provides the cleanest and most sensitive test to theoretical hypotheses. A precise separation of the longitudinal and transverse response functions at $q \geq 1$ GeV/c for light and heavy nuclei may prove helpful in explaining the lack of strength observed at high nucleon momenta.

The y-scaling is very sensitive to the choice of the nuclear form factor, as its very definition clearly implies. If nucleons in the nuclear medium have properties different from the free nucleon, then the electron-nucleon cross section in the nucleus and the value of y will be modified. The

behavior of y-scaling has been investigated as a function of both the size and the mass of the nucleon (104). Figure 18*b* shows that y-scaling in ^{3}He is destroyed by a simultaneous 10% increase of the nucleon size and a 10% decrease of the nucleon mass. Sick (104) concludes for ^{3}He that, if a variation of the radius is correlated with an inverse variation of the mass, the size of the nucleon increases by at most 3%, while if only the size of the nucleon is changed, the maximum increase possible is 6%.

A systematic study (101) of inclusive scattering on a variety of nuclei in the quasielastic scattering region has been carried out recently over a large range of momentum transfers (q = 2–12 fm^{-1}). Day et al (101) showed that y-scaling is also observed for heavy nuclei. The maximum increase of the nucleon radius that is allowed in order to preserve y-scaling in ^{56}Fe is ~3% (104a). This result further reinforces the view that an increase of the nucleon size in heavy nuclei, if present at all, is much smaller than the values that have been proposed (~15%) in order to explain the missing strength in $S_L(q, \omega)$ and the EMC effect.

5.6 *Excitation of the Δ Resonance*

Several inclusive experiments (79, 81, 82, 105) have mapped out the nuclear response for energy transfers ω up to 500 MeV. In these experiments the Δ resonance is as strongly excited as the quasielastic peak. This enables us to study the propagation of the Δ in the interior of nuclei. Since most of our knowledge of the behavior of the Δ resonance in the nucleus comes from pion-nucleus scattering, total photoabsorption and electron scattering provide an additional important test of the theoretical approaches developed for the Δ-N interaction. While the pion-induced reactions are predominantly surface mechanisms, photons and electrons probe the entire nuclear volume. A further advantage of electrons is that q and ω can be varied independently, providing a broader range of investigation of the Δ-nucleus interaction.

O'Connell et al (105) recently studied the Δ resonance in kinematical conditions close to real photoabsorption, $q = \omega$ ($Q^2 = 0$). Data have been obtained on various light nuclei up to ^{16}O. The cross section is found to vary linearly with A, which means that the cross section per nucleon is constant (Figure 19). This agrees with recent experimental results (106–108) obtained for real photoabsorption. The comparison with the electron-proton cross section in the Δ region shows the strong modification of the medium. This is due in particular to the Pauli blocking of the Δ decay, multiple scattering, and the damping of Δ propagation through the ΔN → NN channel. Figure 19 gives the prediction of the Δ-hole approach (109), which has been used successfully to describe photonuclear reactions (110). The pion absorption channel is described by a spreading potential taken from the analyses of pion-nucleus scattering. This calculation reproduces

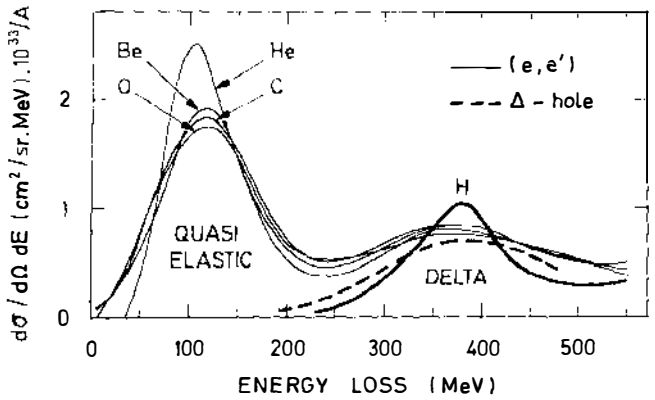

Figure 19 Inclusive cross-section measurements (105) in the isobar region for light nuclei. The dashed curve is the Δ-hole model prediction (109, 110). The thick curve corresponds to the electroexcitation of the free nucleon.

the medium effects reasonably well; however, about 15% of the strength observed experimentally is missing. The spreading potential fitted to pion scattering is not sufficient; more complicated corrections have to be included in the momentum transfer range probed by electron scattering. The failure of the model in the "dip" region between the quasielastic peak and the Δ resonance does not appear to be of fundamental nature. A complete theoretical description of this region is made difficult by the interference with 2p-2h and with higher order contributions from final-state interactions in the quasielastic process (93).

The momentum transfer dependence of the cross section in the Δ resonance region for ^{3}He, ^{12}C, ^{40}Ca, ^{48}Ca, and ^{56}Fe has been studied by Laget (111, 113). He concludes that the resonance contribution seems to be reasonably well understood. His calculations are in better agreement for ^{3}He; this indicates that the disagreement observed might be due to the approximations used for the many-body problem. Especially limiting are the uncertainties and approximations in treating theoretical two-body correlations. The basic mechanism of the excitation of the Δ in the interior of the nucleus appears well understood, but one needs now to perform coincidence experiments to separate the effects of correlations and final-state interactions.

6. PERSPECTIVES FOR THE FUTURE

All the experiments discussed so far were performed at facilities designed in the late 1960s. They reflect both the technological advances and constraints of that era. Intense beams of high energy and tight emittance

effectively employed by high resolution spectrometers made possible the measurements we discussed. On the other hand, the absence of certain classes of data, most notably coincident and polarization transfer data, is a reflection of the limitations of these facilities. Particularly limiting has been their low duty factor (~ 0.01). A high duty factor is essential in coincidence experiments. The unavailability (until quite recently) of polarized electron beams and suitable polarized targets is responsible for the lack of exclusive data in the polarization degrees of freedom.

Both of these limitations were overcome in the early 1980s. Low energy electron scattering facilities with continuous beams (duty factor ≈ 1) have been in operation for the past few years. Polarized beams of high intensity and high degree of polarization (>0.3) also became available at about the same time. Internal polarized targets have been demonstrated to be both feasible and capable of yielding reasonable luminosities when used together with the high intensity beams ($I > 100$ mA) of electron storage rings.

We briefly review in the following two sections some recent results that demonstrate the potential of the new experimental techniques. Recent coincident measurements have probed directly two-nucleon correlations. Experiments with low energy, continuous electron beams have explored phenomena ranging from subthreshold fission to giant resonances. Indicative of the significance attached to coincidence measurements is the fact that every major electron scattering facility under construction, regardless of its maximum energy, is of high duty factor (>0.8).

6.1 *Probing Two-Nucleon Correlations with Coincidence Experiments*

Investigation of two-nucleon correlations requires the coincident detection of two or three reaction products, as in the (e, e′N) or (e, e′2N) channels.

Potentially, two-nucleon knockout experiments (e, e′2N) yield the most direct information on the short-range behavior of the N-N interaction. Such experiments are today at the limits of operating facilities. However, recent results from the ongoing (e, e′p) experiments at low duty factor accelerators have provided evidence for the existence of such correlations.

Coupling of the virtual photon to correlated nucleon pairs was observed in the study of the three-body breakup in the ^{3}He(e, e′p) reaction (112; C. Marchand, private communication). Figure 20 shows three missing energy spectra at recoil momentum values of 316, 401, and 458 MeV/c respectively. The peak at 5.5 MeV corresponds to the one-body knockout reaction to a deuteron final state. A broad peak at higher missing energy values is values of missing energy in each spectrum, is due to the breakup of a p-n pair in ^{3}He. It corresponds to the disintegration of a correlated p-n pair at rest. The curves shown in Figure 20 are the results of a calculation (113)

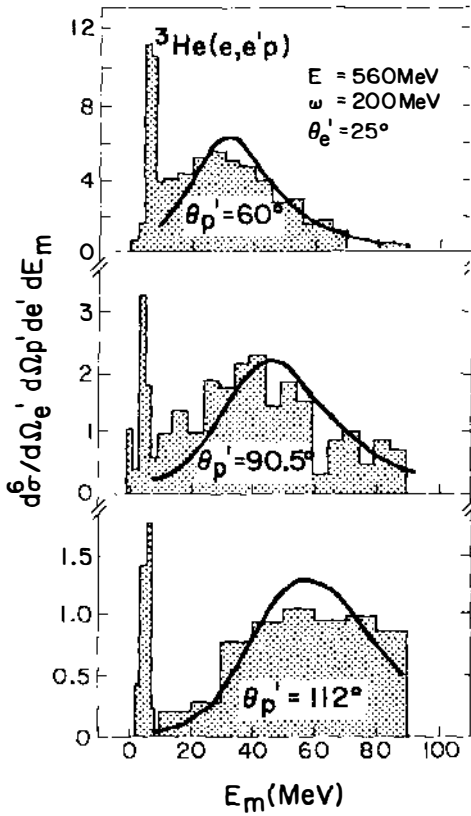

Figure 20 Evidence for the existence of correlated pairs in the ^{3}He(e, e'p) spectra (112; C. Marchand, private communication). The secondary peak is the signature of virtual photon absorption on correlated N-N pairs; the solid curve is a theoretical prediction that includes final-state interactions and meson exchange currents (113).

for ^{3}He based on Faddeev wave functions, a calculation that takes into account final-state interactions and meson exchange currents. Similar (e, e'p) measurements (114) in ^{12}C also find a large increase in the high energy region of the missing mass spectrum.

The ^{3}He(e, e'd)p experiment (115) has allowed the study of two-body mechanisms at low momentum transfers. Cross sections were measured in parallel kinematics with the momentum transfer fixed at $q = 380$ MeV/c and the recoil momentum varying between 0 and 200 MeV/c. The experimental coincidence cross section is shown in Figure 21. The dotted curve is the expected cross section for the process in which the virtual photon couples to a single nucleon. The full curve is obtained if, in addition, the

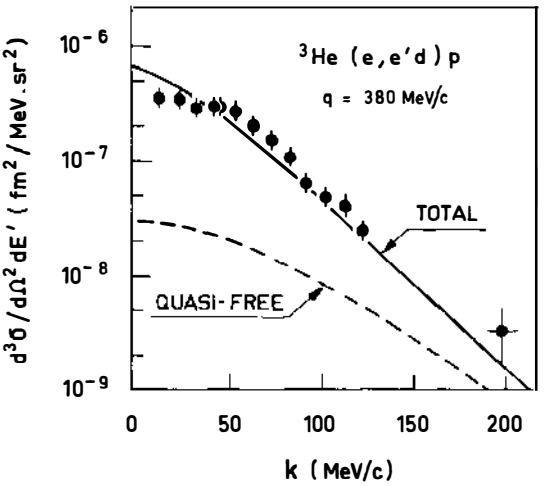

Figure 21 ^{3}He(e,e'd) cross section (115). The dashed curve results from a calculation of quasifree proton knockout. When photoabsorption on correlated n-p pairs, rescattering, and meson exchange effects are included (113), a good description of the data is achieved (*solid curve*).

coupling to a correlated p-n pair is allowed (in either the $T = 0$ or $T = 1$ state).

6.2 *New Facilities: The First Results*

Two major factors have so far limited the power of single-arm electron scattering: (*a*) Excitations in the continuum are broad and overlapping (e.g. giant multipole resonances), and their isolation from the elastic radiative tail, which often accounts for more than 90% of the observed cross section, is problematic. (*b*) The reconstruction of charge and current densities requires knowledge of individual multipole form factors; the single-arm cross section involves the incoherent sum of all multipole form factors allowed by the spin-parity selection rules. It is only in the case of scattering from spin-zero nuclei, and when one single multipole is allowed, that such reconstruction can be performed.

Both of these limitations are removed in coincident electron scattering. The coincidence requirement eliminates the contribution of the elastic radiative tail at the detection stage. The angular pattern of the decay products allows the model-independent determination of multipole strengths and therefore the reconstruction of transition currents and densities. Potentially more powerful is the flexibility that coincidence measurements offer for isolating and studying particular processes that are inaccessible in the inclusive channel.

Coincidence measurements will allow the study of modes of nuclear excitation whose investigation by electron scattering is still rather primitive. A good example is the case of giant resonances, the most important modes of nuclear collective motion. Bulk properties of nuclear and neutron matter, such as compression moduli, symmetry energies, and spin-isospin sound velocity, are derived from their study. Information on the energy dissipation of Fermi liquids can be obtained from the study of their damping (116, 117; J. Wambach, private communication).

The recent ^{208}Pb(e, e′n) measurement (118) exhibits some of the advantages of coincidence electron scattering in the study of continuum excitations. The inclusive spectrum (see Figure 22) is dominated by the elastic radiative tail, but the coincidence spectrum is free of it. In this coincidence measurement, where no angular and energy information from the decay product is retained, the resulting spectra offer the same information as inclusive spectra after the subtraction of the radiative tail. Multipole strength functions were extracted by a multipole decomposition analysis of the combined (e, e′n) and (γ, n) data. The resulting monopole-quadrupole

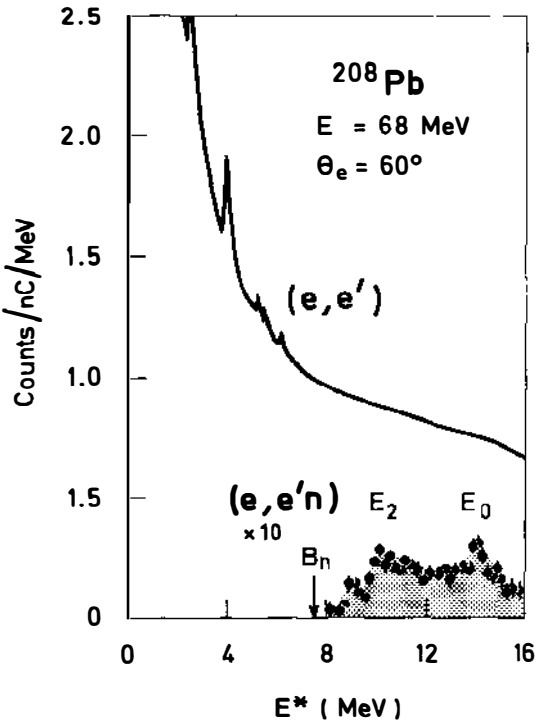

Figure 22 Single-arm and coincident (e, e′n) spectra from ^{208}Pb (118). The coincidence condition removes the radiative tail, revealing the excitation of giant resonances.

strength function exhibits two resonant structures at 10.6 and 14.1 MeV, as evident in the coincidence spectrum (see Figure 22). The integrated strength between 9 and 12.5 MeV exhausts 65% of the energy-weighted quadrupole sum rule, the strength between 12.5 and 16 MeV will satisfy 130% of the isoscalar EWSR. These results are in good agreement with the HF-RPA predictions (117) and have definitively settled previous contradictory statements from different experiments. The ability of mean field theory to describe these very important collective modes of excitation of the nuclear many-body system is thus demonstrated to be as good as in the case of the nuclear charge densities and low frequency excitations discussed in Section 4.

As coincidence measurements become more exclusive, the power of the (e, e′x) probe to isolate particular channels and to yield microscopic information is greatly enhanced. In the study of the ^{28}Si(e, e′p) reaction (119), the energy spectrum of the emitted particles allows the isolation of the decay to the ground state and various excited states of the daughter nucleus. The study of the angular distribution of the decay to any of these states then provides the most complete result of a two-arm coincidence measurement. The angular distribution of the α decay of ^{28}Si to the ground state of ^{24}Mg shown in Figure 23. It has allowed determination of multipole

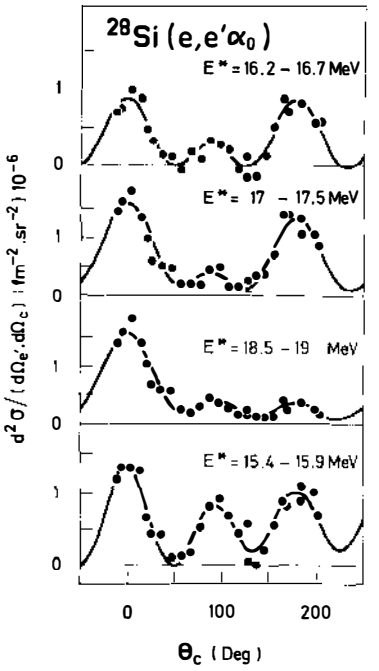

Figure 23 Angular distributions from the ^{28}Si(e, e′α)^{24}Mg coincidence measurements (119).

strengths. The derived E1 strength agrees with the corresponding photodisintegration experiment. The deduced E2/E0 strength amounts to 42% of the E2 sum rule, twice the value derived from isoscalar probes, which indicates the presence of strong isovector E2/E0 excitations.

In the (e, e′γ) reaction both the excitation and decay channels are electromagnetic, and therefore free of final-state hadronic interactions. It can be used in the study of both reaction (e.g. radiative corrections) and structure questions. Its most obvious use is in the study of bound states of non-zero-spin nuclei (120, 121). The angular pattern of the decay gamma rays allows the determination of individual multipole form factors for excited states of non-zero-spin nuclei, which in turn facilitates the reconstruction of the corresponding transition charge densities.

The first nuclear structure investigation utilizing (e, e′γ) was performed on the 4.4-MeV state of ^{12}C (120). This state had been previously studied by inclusive inelastic scattering, and the two form factors involved (F_T, transverse, and F_L, longitudinal) were isolated through the Rosenbluth method. The (e, e′γ) reaction provides an alternative way of separating them through the measurement of their interference and at the same time reveals their relative sign. If $|F_T|^2$ were zero, a simple quadrupole pattern relative to the q axis would result. The effect of a nonvanishing F_T is to rotate the pattern with respect to the q axis; the sense of rotation is clockwise if F_T and F_L have the same sign, and counterclockwise if they have opposite signs. A counterclockwise rotation was observed (see Figure 24), which means the relative sign was negative. This phase is in agreement

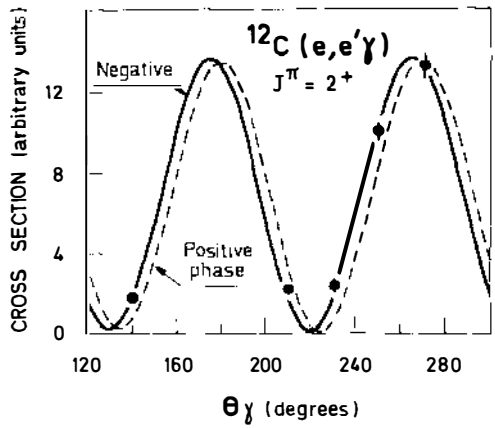

Figure 24 Angular distribution from the ^{12}C(e, e′γ) experiment (120). It allows the separation of the two contributing multipoles (C2 and E2) and determination of their relative phase.

with theory, which predicts that the transverse form factor is dominated by the convection current at low momentum transfers.

The increase in energy at electron accelerators with high duty factor will allow the study of these phenomena at a much wider dynamic range of momentum transfers. At higher energy, the same coincidence techniques, applied now to giant resonances, can be used for the investigation of nucleon resonances. The comparison of the transition currents of nucleon resonances studied in the proton and finite nuclei can provide precise and discriminating evidence of the influence of the nuclear medium on the intrinsic properties of the nucleon.

The drawbacks inherent to the standard setup of external beam–fixed targets are numerous: inability to study short-lived isotopes, degradation of the energy spectrum caused by straggling of particles emerging from the target, and difficulty in maintaining target polarization due to beam heating are among them. In a pioneering series of experiments at Novosibirsk, gas jet targets have been used in the VEPP-3 electron ring (122; S. C. Popov, private communication). The intense circulating electron beam ($I \approx 300$ mA) compensates for the very thin targets and results in reasonable luminosities.

Figure 25 shows the data obtained in the first internal target experiment reported, that of ^{16}O(e, e′x). Except for the internal target, the experimental arrangement is quite conventional: an electron spectrometer and decay particle detectors surround the interaction region. The quality of the data is impressive. Clearly, backgrounds are under control and worries regarding the feasibility of operating the ring and of obtaining high quality data in such an environment have been alleviated.

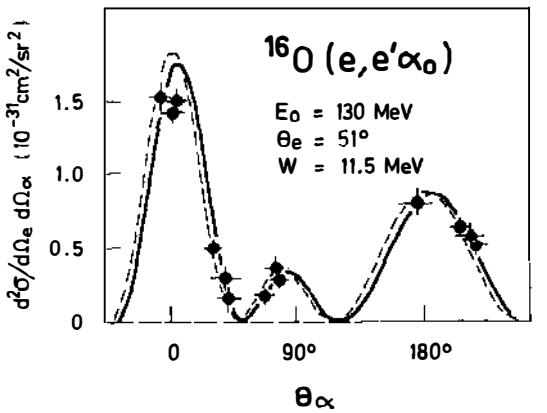

Figure 25 Coincidence electron scattering data from ^{16}O obtained in the depicted internal jet target setup of Novosibirsk (122).

Already the same group has reported electron scattering measurements from a polarized deuterium jet target (123). The possibilities offered by such measurements are numerous and exciting.

7. CONCLUSION

Recent electron scattering experiments have provided a wealth of new information on nuclear structure. The interpretation of the experimental results in the two- and three-body systems requires the explicit treatment of nonnucleonic degrees of freedom. Mesonic degrees of freedom are sufficient to account for the observed discrepancy between the nucleonic description and experiment up to $Q^2 \approx 25\,\mathrm{fm}^{-2}$. The role of the pion is well understood up to $\sim 15\,\mathrm{fm}^{-2}$. The modification of the intrinsic properties of the nucleon inside the nucleus appears to be less significant than originally suggested. The suppression of the longitudinal quasifree response appears to be induced mostly by many-body correlations. Discrepancies remain, which suggests that other effects are also contributing. Further experimental and theoretical investigations are needed.

The concept of nucleons moving in a mean field has been found to be valid throughout the nuclear volume by determining the charge distribution of the 3s orbit in lead. Yet the precise determination of ground and transition charge densities has shown that mean field theories using effective interactions cannot describe the interior structure of nuclei. Elastic charge and magnetic scattering and the study of a variety of other inelastic excitations in the lead region have shown that correlations reduce occupation probabilities by $\sim 30\%$ for valence orbitals.

In the last few years a noticeable transition to more exclusive measurements has been taking place. Coincident (e, e′p) studies in the quasifree region yield precise information on the momentum distributions of nucleons in the nucleus. These experiments recently provided for the first time direct evidence for two-body correlations. However, little is known about short-range processes.

The first results from continuous-beam electron accelerators have demonstrated, at low energies, the feasibility and the importance of coincidence measurements. Continuum excitations (especially giant multipole resonances) are now being studied with a precision previously restricted to bound states. The feasibility of isolating multipole form factors in mixed transitions through the (e, e′γ) reaction has been demonstrated. The study of nucleon resonances in nuclei, using these same coincidence techniques at higher energy, appears promising. The experimental method has been further widened by the use of internal polarized targets in coincidence measurements.

Quantum chromodynamics (QCD) has emerged as the fundamental theory of strong interactions, and in the asymptotic limit of short distances it successfully defines the desired behavior of any nuclear model, just as the traditional approach does in the limit of large distances. Yet, QCD remains intractable in the strong coupling regime, and the problem of confinement is still unsolved. A unified description of these two phases of hadronic matter within a general framework, based on fundamental theory, has emerged as one of the key tasks confronting nuclear physics (124).

Experimental data exploring the transition region between confinement and asymptotic behavior are needed to provide guidance to theory. The success of the previous generation of electron scattering facilities combined with the versatility and precision of the continuous-beam electron accelerators has led the nuclear community in the US to declare as its highest priority the construction of a multi-GeV electron accelerator suitable for coincidence and polarization studies. This goal is being realized by the construction of the Continuous-Beam Electron Facility (CEBAF) in Virginia (125). CEBAF will be augmented by lower energy, continuous-beam electron accelerators that will further explore the mesonic and collective degrees of freedom. Similar plans and construction projects are also being undertaken in Europe (125). The availability of these facilities in the early 1990s will bring the study of nuclei with electromagnetic probes to a new era.

ACKNOWLEDGMENTS

We would like to express our deep appreciation for the many ideas, criticisms, and suggestions we have received from the electron scattering community and nuclear structure theorists. We are particularly indebted to our colleagues at Illinois and Saclay. An attempt to give even a partial list of people who have substantially contributed to this review would be prohibitively long. This work was supported in part by the National Science Foundation under grant NSF PHY 86-10493 and by a CNRS-NSF exchange program under grant NSF INT 83-12952.

Literature Cited

1. Donnelly, T. W., Sick, I. *Rev. Mod. Phys.* 56: 461 (1984)
2. Frullani, S., Mougey, J. *Adv. Nucl. Phys.* 14: 1 (1984)
3. Heisenberg, J., Blok, H. *Ann. Rev. Nucl. Part. Sci.* 33: 569 (1983)
4. Aubert, J. J., et al. *Phys. Lett.* 123B: 275 (1983)
5. Drechsel, D. *Prog. Part. Nucl. Phys.* 13: 64 (1984)
6. Ciofi degli Atti, C. *Prog. Part. Nucl. Phys.* 3: 163 (1980)

7. DeForest, T. Jr., Walecka, J. D. *Adv. Phys.* 15: 1 (1966)
8. Amaldi, E., Fubini, S., Furlan, G. *Pion Electro-production.* Berlin: Springer (1979)
9. Villars, F. *Helv. Phys. Acta* 20: 476 (147)
10. Chemtob, M., Rho, M. *Nucl. Phys.* A163: 1 (1971)
11. Riska, D. O., Brown, G. E. *Phys. Lett.* 38B: 193 (1972)
12. Rho, M. *Ann. Rev. Nucl. Part. Sci.* 34: 531 (1984)
13. Auffret, S., et al. *Phys. Rev. Lett.* 55: 1362 (1985); Simon, G., et al. *Nucl. Phys.* A324: 277 (1979) and references therein
14. Leidemann, W., Arenhövel, H. *Nucl. Phys.* A393: 385 (1983)
15. Mathiot, J. F. *Nucl. Phys.* A412: 201 (1984)
16. Brown, G., Rho, M., Weise, W. *Nucl. Phys.* A454: 669 (1986)
17. Riska, D. O. *Phys. Scripta* 31: 471 (1985); Buchmann, A., Leidemann, W., Arenhövel, H. *Nucl. Phys.* A443: 726 (1985)
18. Brown, G., Rho, M. *Comments Nucl. Part. Phys.* 10: 210 (1981)
19. Kisslinger, L. *Lect. Notes Phys.* 260: 432 (1986) and references therein
20. Yamauchi, Y., Yamamoto, R., Wakamatsu, *M. Phys. Lett.* 146B: 153 (1984)
21. Arnold, R. G., et al. *Phys. Rev. Lett.* 58: 1723 (1987)
22. Auffret, S., et al. *Phys. Rev. Lett.* 54: 649 (1985)
23. Cramer, R., et al. *Z. Phys.* C29: 513 (1985) and references therein
24. Gari, M., Hyuga, H. *Nucl. Phys.* A264: 409 (1976)
25. Sitarski, W. P., Blunden, P., Lomon, E. L. To be published
26. Hoehler, G., et al. *Nucl. Phys.* B114: 505 (1975)
27. Zuilhof, M. J., Tjon, J. A. *Phys. Rev.* C22: 2369 (1980)
28. Arnold, R. G., Carlson, C. E., Gross, F. *Phys. Rev.* C21. 1426 (1980)
29. Chemtob, M., Furui, S. *Nucl. Phys.* A454: 548 (1986)
30. Takeuchi, S., Yazaki, K. *Nucl. Phys.* A438: 605 (1985)
31. Nyman, E. N., Riska, D. O. *Phys. Rev. Lett.* 57: 3007 (1986)
32. Martino, J. *Lect. Notes Phys.* 260: 129 (1986)
33. Friar, J. L., Gibson, B. F., Payner, G. L. *Ann. Rev. Nucl. Part. Sci.* 34: 403 (1984) and references therein
34. Sasakawa, T., Ishikawa, S. *Few Body Systems* 1: 3 (1986)
35. Hajduk, C., Sauer, P., Strueve, W. *Nucl. Phys.* A405: 620 (1983)
36. Juster, F. P., et al. *Phys. Rev. Lett.* 55: 2261 (1985) and references therein; Beck, D. *PhD thesis,* MIT (1986)
37. Carlson, J., Pandharipande, V. R., Wiringa, R. B. *Nucl. Phys.* A401: 59 (1983)
38. Hadjimichael, E., Goulard, B., Bornais, R. *Phys. Rev.* C27: 831 (1983)
39. Beyer, M., Drechsel, D., Giannini, M. M. *Phys. Lett.* 122B: 1 (1983); Hoodboy, P., Kisslinger, L. *Phys. Lett.* 146B: 163 (1984)
40. Maize, M. A., Kim, Y. E. *Phys. Rev.* C35: 1060 (1987); Vary, J. P., Coon, S. A., Pirner, H. J. In *Few Body Problems in Physics,* Vol. II, ed. B. Zeitnitz. Amsterdam: North Holland (1986)
41. Tjon, J. A. *Nucl. Phys.* A446: 173c (1985)
42. Dunn, P., et al. *Phys. Rev.* C27: 71 (1983); Otterman, C., et al. *Nucl. Phys.* A436: 688 (1985); Cavedon, J. M., et al. *Phys. Rev. Lett.* 49: 986 (1982) and references therein
43. Strueve, W., Hajduk, C., Sauer, P. *Nucl. Phys.* A405: 620 (1983)
44. Riska, D. O. *Nucl. Phys.* A350: 227 (1980)
45. Maize, M. A., Kim, Y. E. *Nucl. Phys.* A420: 365 (1984)
46. Friar, J. L., Negele, J. W. *Adv. Nucl. Phys.* 8: 219 (1975)
47. Frois, B., et al. *Phys. Rev. Lett.* 38: 152 (1977)
48. McCarthy, J. S., Sick, I., Whitney, R. R. *Phys. Rev.* C15: 1396 (1977)
49. Emrich, J., et al. *Nucl. Phys.* A396: 401c (1983)
50. Sick, I., et al. *Phys. Lett.* 88B: 245 (1979)
51. Reuter, W., et al. *Phys. Rev.* C26: 806 (1982)
52. Cardman, L. S., et al. *Phys. Lett.* 91B: 203 (1980)
53. Dechargé, J., Gogny, D. *Phys. Rev.* C21: 1568 (1968)
54. Gogny, D. *Lect. Notes Phys.* 108: 88 (1979)
55. Dechargé, J., Sips, L. *Nucl. Phys.* A407: 1 (1983)
56. Buti, T. N., et al. *Phys. Rev.* C33: 755 (1986)
57. Deleted in proof
58. Wise, J. E., et al. *Phys. Rev.* C31: 1699 (1985)
59. Deleted in proof
60. Goutte, D., et al. *Phys. Rev. Lett.* 45: 1618 (1980)
61. Deleted in proof

62. Euteneuer, H., Friedrich, J., Voegler, N. *Nucl. Phys.* A298: 452 (1978)
63. Cavedon, J. M., et al. *Phys. Rev. Lett.* 49: 978 (1982)
64. Frois, B., et al. *Nucl. Phys.* A396. 409c (1983)
65. Papanicolas, C. N., et al. *Phys. Rev. Lett.* 58: 2296 (1987)
66. Platchkov, S., et al. *Phys. Rev.* 25. 2318 (1982)
67. Suzuki, T., et al. *Phys. Rev.* C26: 750 (1982)
68. Suzuki, T., Hyuga, H. *Nucl. Phys.* A204: 491 (1983)
69. Pandharipande, V. R., Papanicolas, C. N., Wambach, J. *Phys. Rev. Lett.* 53: 1133 (1984)
70. Fantoni, S., Pandharipande, V., R. *Nucl. Phys.* A427: 473 (1984)
71. Mahaux, C., et al. *Phys. Rep.* 120C: 1 (1985)
72. Quint, E., et al. *Phys. Rev. Lett.* 57: 186 (1986); 58: 1727 (1987)
73. Jaminon, M., Mahaux, C., Ngô, H. *Phys. Lett.* 158B: 103 (1985)
74. Cavedon, J., et al. *Phys. Rev. Lett.* 58: 195 (1987)
75. Whitney, R. R., et al. *Phys. Rev.* C9: 2330 (1974)
76. Moniz, E. J., et al. *Phys. Rev. Lett.* 26: 445 (1971)
77. Horikawa, Y., et al. *Phys. Rev.* C22: 1680 (1980)
78. Altemus, R., et al. *Phys. Rev. Lett.* 44: 965 (1980)
79. Barreau, P., et al. *Nucl. Phys.* A402: 515 (1983)
80. Deady, M., et al. *Phys. Rev.* C28: 631 (1983)
81. Meziani, Z. E., et al. *Phys. Rev. Lett.* 52: 2130 (1984); 54: 1233 (1985)
82. Marchand, C., et al. *Phys. Lett.* 153B: 29 (1985)
83. Blatchley, C. C., et al. *Phys. Rev.* C34: 1243 (1986)
84. DeForest, T. Jr. *Nucl. Phys.* A414: 347, 358 (1984)
84a. McVoy, K. W., Van Hove, L. *Phys. Rev.* 125: 1034 (1962)
85. Schiavilla, R., et al. *Preprint ILL-(NU)-86-60*, to be published
86. Do Dang, G., Van Giai, N. *Phys. Rev.* C30: 731 (1984)
87. Walecka, J. D. *Ann. Phys. NY* 83: 491 (1974); Serot, B. D., Walecka, J. D. *Adv. Nucl. Phys.* 16: 1 (1986)
88. Kurasawa, H., Suzuki, T. *Phys. Lett.* 154B: 6 (1985)
89. Noble, J. *Phys. Rev. Lett.* 46: 412 (1981)
90. Celenza, L. S., et al., *Phys. Rev.* C31: 232 (1985)
91. Traini, M. *Phys. Lett.* B176: 266 (1986)
92. Deleted in proof
93. Alberico, W., et al. *Ann. Phys.* 154: 356 (1984)
94. Cavinato, M., et al. *Nucl. Phys.* A423: 376 (1984)
95. Della Fiore, A., et al. *Phys. Rev.* C31: 1088 (1985)
96. Orlandini, G., Traini, M. *Phys. Rev.* C32: 320 (1985)
97. Fantoni, S., Pandharipande, V. *Preprint ILL-(NU)-86-52*, to be published
98. West, G. B. *Phys. Rep.* 18C: 264 (1975)
99. Gurvitz, S., Tjon, J., Wallace, S. *Phys. Rev.* C34: 648 (1986); Ciofi degli Atti, C. *Nucl. Phys.* A463: 127c (1987)
100. Sick, I., Day, D., McCarthy, J. S. *Phys. Rev. Lett.* 45: 871 (1980)
101. Day, D., et al. To be published
101a. Ciofi degli Atti, C., Pace, E., Salwe, G. Phys. Lett. 127B: 303 (1983)
102. Jans, E., et al. *Phys. Rev. Lett.* 49: 974 (1982)
103. Laget, J. M. *Phys. Lett.* 151B: 325 (1985)
104. Sick, I. *Phys. Lett.* 157B: 13 (1985)
104a. Sick, I. See Ref. 124
105. O'Connell, J. S., et al. *Phys. Rev. Lett.* 53: 1627 (1984)
106. Arends, J., et al. *Phys. Rev. Lett.* 98B: 423 (1981)
107. Ahrens, J., et al. *Phys. Lett.* 146B: 303 (1984)
108. Carlos, P., et al. *Nucl. Phys.* A431: 573 (1984)
109. Koch, J. H., Ohtsuka, N. *Nucl. Phys.* A435: 765 (1985)
110. Koch, J. H., Moniz, E. J., Ohtsuka, N. *Ann. Phys. NY* 154: 99 (1984)
111. Laget, J. M. *Phys. Rep.* 69: 1 (1981)
112. Marchand, C. *Phys. Lett.* 153B: 29 (1985)
113. Laget, J. M. In *New Vistas in Electronuclear Physics*, ed. E. L. Tomusiak, H. S. Caplan, E. T. Dressler, p. 361. New York: Plenum (1986)
114. Lourie, R. W., et al. *Phys. Rev. Lett.* 56: 2364 (1986)
115. Keizer, P. W. M., et al. *Phys. Lett.* 157B: 255 (1985)
116. Bertsch, G. F., Bortignon, P. F., Broglia, R. *Rev. Mod. Phys.* 55: 287 (1983)
117. Wambach, J. In *Proc. Int. Sch. Nucl. Struc.*, ed. V. G. Soloviev, P. Yu. Popov. Aluhsta, USSR (1986)
118. Bolme, G., et al. To be published; Cardman, L. S. In *Proc. Int. Sch. Intermediate Energy Nucl. Phys.*, ed. R. Bergere, S. Costa, C. Schaerf, p. 163. Singapore: World Sci. (1986)

119. Kihm, Th., et al. *Phys. Rev. Lett.* 56: 2789 (1986)
120. Papanicolas, C. N. *Phys. Rev. Lett.* 54: 26 (1985)
121. Ravenhall, D. G., et al. *Ann. Phys.* In press (1987)
122. Popov, S. C. *Proc. Workshop on the Use of Electron Rings for Nucl. Phys. Res., Univ. Lund*, 2: 150 (1982); Dmitriev, V. F., et al. *Nucl. Phys.* A464: 237 (1987)
123. Dmitriev, V. F., et al. *Phys. Lett.* 157B: 143 (1983)
124. Walecka, J. D. In *Proc. Symp. Celebrating 35 Years of Electron Scattering*, ed. C. N. Papanicolas, L. S. Cardman, R. A. Eisenstein. *AIP Conf. Ser.* In press (1987)
125. Grunder, H. See Ref. 124